SATE

Systems & Advanced Technologies Engineering S.r.l.

N-TOF TARGET #3

FLOW INDUCED VIBRATION ANALYSIS OF THE ANTI-CREEP PLATES

Phase 1 - Final report

Client: CERN

Document N°.: 610003-REP-WP4-T001- Rev. 1

Copy _1_ of _1_

Date: 09-01-2019

Pages: 43 + 1 Ann.

Authors:
Ing. Attilio Brighenti

Checked:
Ing. Attilio Brighenti

Authorised:
Ing. Attilio Brighenti

DISTRIBUTION:

CERN

1 electronic copy (pdf)

Systems & Advanced Technologies Engineering S.r.l.

REVISION SHEET

Sheet	1	2	3	4	5	6	7	8	9	10	11	12	13	14	15
Rev.	0	0	0	0	0	0	0	0	0	0	0	0	0	0	0
Sheet	16	17	18	19	20	21	22	23	24	25	26	27	28	29	30
Rev.	0	0	0	1	0	0	0	1	0	0	0	0	0	0	0
Sheet	31	32	33	34	35	36	37	38	39	40	41	42	43		
Rev.	0	1	0	0	0	0	0	0	0	0	0	0	0		
Annex	A1														
Rev.	0														

Document history

Rev.	Date of issue	Description
0	30/11/2018	Issue for approval
1	09/01/2019	Corrected section heading style and typo errors

Changes other than typing/grammar proofing, brought with Rev. x, are marked by the following annotation on the right margin and shaded in yellow.

Rev. x

LIST OF CONTENTS

ANNEXES

1 SCOPE

This document is the final report of the first phase of a study intended to preliminarily check if flow induced vibrations (FIV) can arise due to lock-on among vortex excited at side opening of cavities facing the fluid flow through the main tube of the n-Tof Target # 3 cradle.

The activities performed and reported are consistent with the SoW under Ref. 3.5.1, object of the order nr. CA7459608 by CERN dtd. 05/10/2018.

2 SUMMARY AND CONCLUSIONS

2.1 Main results

The potential vortex frequency at the cradle ports openings span a range from about 130 Hz to about 2 kHz, depending on the operating condition (A or B) and on the port, out of the five channels rows, at the base case pressure (1 atm absolute). See as an example Fig. 1, relevant to condition B.

However only in some of them the Reynolds number exceeds the minimum value (10^5) needed to power self-excited standing waves by lock-on of acoustic modes, when theoretical frequencies match.

Moreover, above a certain grazing speed none of the three base acoustic modes considered (Helmholtz cavity, 1st and 2nd channels modes) would be locked to the vortex frequencies.

This restricts the potential acoustic-vortex lock-on frequencies to the range between about 500 Hz and 1.6 kHz in the base case pressure.

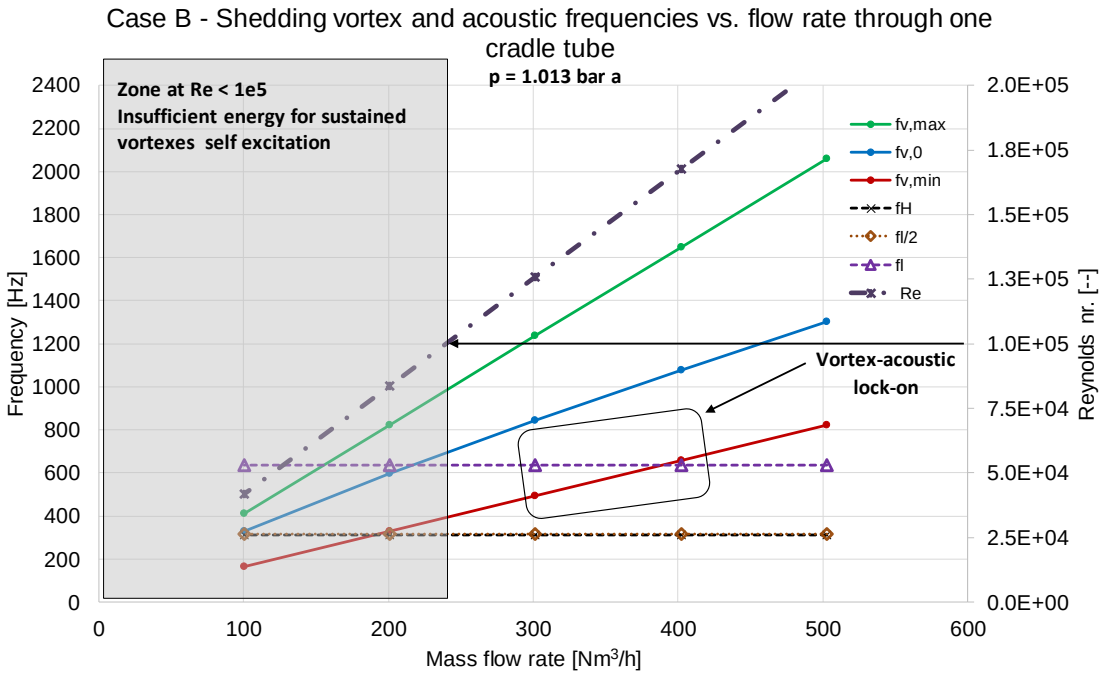

Fig. 1 – Synthesis of Case B at 1 atm pressure

Only the acoustic resonance of the one wave length mode ($L = \lambda$) of the vertical channel (at 635 Hz) could be excited by shed vortexes, limited to the first two anti-creep plates channels sets downstream the inlet of the cooling gas, in the operating case A, or limited to the 2nd and 3rd channel sets, in the operating case B (at the base case pressure).

In no case the first ten structural modes of the anti-creep plates reported by CERN can lock-on to the above acoustic frequencies, since their maximum frequency (10th mode) is at about 318 Hz, thus far enough from the acoustic resonances.

The results for the two other pressures, 0.9 and 1.1 atm abs., do not change substantially the above conclusions. The worse condition occurs, however, at the higher pressure for case B in which the first three anti-creep plate channels can resonate at the highest acoustic mode (635 Hz).

2.2 Recommendations

The present preliminary study is based on some simplifying assumptions, namely:

a. the constant density and speed of sound along the acoustic paths. This is not totally true as the gas expands while heating up while flowing through the anti-creep plate channels. However, the expansion ratio, as reported by the Client is relatively small and its effects are sufficiently covered by the sensitivity analysis performed.
b. stand-alone Helmholtz cavities and channels models, i.e. with no mutual interaction by broader modal patterns. This, however does not hide possible lock-on of combined acoustic modes (i.e. spanning two or more channels), because these would have higher standing wave lengths, thus lower frequencies than those here obtained. In particular they would be lower than the vortex frequency range, and could match only at Reynolds numbers lower than the minimum needed to have enough power for self-sustained pulsations.

These simplifications, therefore, upon SATE opinion, do not bias the conclusion that ***none of the first 10 structural modes are excited by vortexes locked-on to any acoustic modes***, based on the sensitivity analysis performed among the various ports and the absolute pressure values explored (1 ± 0.1 atm).

Instead, it is recommended to investigate and evaluate the potential matching of the structural modes beyond the 10th, taking into account not only the frequency match but also the pressure field and displacement shapes coupling between the acoustic modes and the structural ones.

3 DEFINITIONS AND REFERENCE DOCUMENTS

3.1 Abbreviations and Definitions

The following definitions are applied within this document.

AIV	Acoustic Induced Vibration
Client/Contractor	CERN
FIV	Flow Induced Vibration
MoM	Minute of Meeting(s)
Subcontractor	S.A.T.E. - Systems & Advanced Technologies Engineering S.r.l. – Venice

3.2 Symbols

Symbol	Description	Units
	Geometrical data	
D_p	Header pipe inner diameter	[mm]
L_{ap}	Anti-creep plate channels length (average along flow)	[mm]
b_{ap}	Anti-creep plate channels gap (between ribs)	[mm]
t_{ap}	Anti-creep plate channels thickness (across flow)	[mm]
n_{ap}	Number of channels per Anti-creep plate	[--]
V_{pl}	Anti-creep plate cavity plenum volume (approx.)	[mm^3]
V_c	Anti-creep plate cavity total volume	[mm^3]
L_c	Cavity width (along cradle header pipe flow)	[mm]
$d_{c,eq}$	Cavity equivalent diameter, for $f_v(St)$	[mm]
b_c	Cavity breadth at the cradle header pipe ports	[mm]
r_c	Cavity edge radius (upstream side)	[mm]

Symbol	Description	Units
A_c	Cavity neck section area	[mm^2]
l_{cp}	Cavity neck perimeter	[mm]
H_c	Cavity neck thickness (Cradle header pipe thickness)	[mm]
H_a	Cavity neck added thickness (fluid stream tube extension)	[mm]
	Fluid and operating data	
mfr	Mass flow rate in feed pipe	[Nm^3/h] [kg/s]
T	Temperature	[°C]
p	Pressure	[bar a]
p'	Pressure pulsation amplitude	[bar a]
μ	Molar mass	[kg/kmole]
z	Compr. factor	[--]
ρ	Density	[kg/m^3]
η	Absolute viscosity	[Pa s]
ν	Kinematic viscosity	[m^2/s]
γ	Specific heat ratio	[--]
c_s	Speed of sound	[m/s]
	Vorticity calculations at cradle tube ports	
U_0 or v_0	Mean grazing flow velocity in front of the cavity	[m/s]
Re	Reynolds number	[--]

Symbol	Description	Units
Ma	Mach number	[--]
St_1	Low Re Strouhal number	[--]
St_2	High Re Strouhal number	[--]
St	Matching Strouhal number	[--]
$f_{v,0}$	**Central vortex frequency**	[Hz]
$f_{v,min}$	Min vortex frequency	[Hz]
$f_{v,max}$	Max vortex frequency	[Hz]
	Acoustic resonance calculations	
f_H	**Helmholtz acoustic frequency**	[Hz]
AM_H *(center)*	Acoustic Margin (from Central vortex frequency)	[--]
ALO_H	Lock-on condition ($0.8 * f_{v,min} < f < 1.2 * f_{v,max}$) AND ($Re > Re_{min}$)	[--]
$f_{\lambda/2}$	**1st channel acoustic mode**	[Hz]
$AM_{\lambda/2}$ *(center)*	Acoustic Margin (from Central vortex frequency)	[--]
$ALO_{\lambda/2}$	Lock-on condition ($0.8 * f_{v,min} < f < 1.2 * f_{v,max}$) AND ($Re > Re_{min}$)	[--]
f_{λ}	**2nd channel acoustic mode**	[Hz]
AM_{λ} *(center)*	Acoustic Margin (from Central vortex frequency)	[--]
ALO_{λ}	Lock-on condition ($0.8 * f_{v,min} < f < 1.2 * f_{v,max}$) AND ($Re > Re_{min}$)	[--]
	Structural modes	
$f_{s,1...\nu}$	Mode 1…n	[Hz]

3.3 Client reports, specifications and E-mails

1. CERN Rui Ximenes EN-STI "n-Tof Target #3 - Vibration analysis meeting with SATE" (12/09/2018), file: n_TOF_Target3_vibration_analysis_meeting_w_SATE.pdf.
2. CERN Rui Ximenes EN-STI "RE: Videoconferenza w/ SATE per analisi vibrazione n_TOF Target #3" (21/09/2018 15:58), file: Vibration Modes.zip.
3. CERN Rui Ximenes EN-STI "n-Tof Target #3 - Flow Induced Vibration support documentation from CERN" (16/10/2018), file: n_TOF_Target_(CERN)_Support file.pdf.

3.4 Client Drawings

1. TOFTARTF3P_0082 “Anti-creep plate”, dated 2018-10-12 (file: n_TOF_Target_(CERN)_Anti-creep plate 2D.pdf).
2. n_TOF_Target_(CERN)_Assembly 3D.stp
3. n_TOF_Target_(CERN)_N2 Volume.stp
4. n_TOF_Target_(CERN)_N2 Volume-simplified.stp

3.5 SATE reports, specifications and E-mails

1. SATE document: “n-Tof Target #3 – flow induced vibration (FIV) analysis of the ani-creep plates - technical and commercial proposal”, ref. 32/2018, dated 24 September 2018
2. 610003-REP-WP4-T001 – “n-Tof Target #3 - Preliminary Flow Induced Vibration analysis – detailed calculations”, rev. 0 dated 14/11/2018 (included as Annex A1herewith).

3.6 Other references

1. M. S. Howe: “Contributions to the theory of aerodynamic sound with applications to excess jet noise and the theory of the flute”, 1975 Journal of Fluid Mechanics 71(4), 625–673.
2. M. S. Howe: “On the absorption of sound by turbulence and other hydrodynamic flows” 1984 Journal of Applied Mathematics 32, 187–209.
3. Junkowski W.M., Botros K.K., Studzinski W.: " Cyindrical side-branch as tone generator" Journal of Sound and Vibration (1989) 131(2), 265-285.
4. Miller D.S.: “Internal flow systems”, 2nd ed. (1990) Publ. by BHR Group Ltd.
5. Pipeline and Compressor Research Council (PCRC): “Controlling the effects of pulsations and fluid transients in industrial plants – Pulsation & vibration short course”, February 1991.
6. Bruggeman J.C. et al.: “Self-sustained aero-acoustic pulsations in gas transport systems: experimental study of the influence of closed side branches”, Journal of Sound and Vibration (1991), 150(3), 371-393.
7. Rogers L.E.: “Design stage acoustic analysis of natural gas piping systems in centrifugal compressor stations”, International gas turbine and aeroengine congress and exposition, ASME 1991, 91-GT-238.
8. ISO 10816-1:1995/Amd 1:2009: “Mechanical vibration - Evaluation of machine vibration by measurement on non-rotating parts - part 1 General guidelines”.

9. Ziada S., Shine S.: "Strouhal numbers of flow-excited acoustic resonance of closed side branches", Journal of Fluids and Structures (1999) 13, 127-142.
10. Peters M., van Bokhorst E.: “Flow induced pulsations in pipe systems with closed branches, impact of flow direction”, Flow Induced Vibrations, Ziada &Staubli (esd) 2000 Balkema, Rotterdam ISBN 90 5809 129 5.
11. Dequand S., Hulshoff S.J., Hirschberg A.: “Self-sustained oscillations in a closed side branch system”, Journal of Sound and Vibration (2003), 265, 359-386.
12. Hemon P., Santi F., Amandolèse X.: "On the pressure oscillations inside a deep cavity excited by a grazing airflow" European Journal of Mechanics B/Fluids 23 (2004) 617-632.
13. Amandolèse X., Hemon P., Santi F.: "An experimental study of the acoustic oscillations by flow over cavities" Transactions of the ASME Vol. 126, pp 190-195, April 2004.
14. Ziada S., Scott S., Arthurs D.: "Acoustic excitation by flow in T-junctions", Transactions of the ASME (2007) 129, 14-20.
15. Peters R.: “Acoustic wave theory - fundamentals of acoustics - wave propagation in piping”, TNO TPD PVC Workshop 2008.
16. Energy Institute, “Guidelines for the Avoidance of Vibration Induced Fatigue Failure in Process Pipework”, 2nd edition January 2008, Energy Institute, London.
17. Zugno F.: "Fenomeni di instabilità aeroacustica in corrispondenza di diramazioni cieche in condotte per il trasporto del gas naturale", Master degree thesis in collaboration under stage at SATE S.r.l. - Univ. of Padua, 2008-2009.
18. API RECOMMENDED PRACTICE 688 “Pulsation and Vibration Control in Positive Displacement Machinery, Systems for Petroleum, Petrochemical, and Natural Gas Industry Services”, 1st Ed., April 2012.
19. Kalpakli Vester A.: ”Vortices in turbulent curved pipe flow-rocking, rolling and pulsating motions”, Technical Reports from Royal Institute of Technology KTH Mechanics SE–100 44 Stockholm, Sweden, May 2014.
20. NIST Standard Reference Database 23: https://www.nist.gov/publications/nist-standard-reference-database-23-nist-thermodynamic-and-transport-properties-refprop.

4 INTRODUCTION TO FIV

4.1 Premise

Flow induced and acoustic induced vibrations, respectively FIV and AIV, are recognised as a problem to be prevented in several types of industrial systems and vehicles.

In process plants they can induce piping and supports fatigue and rupture in very short time (from minutes to days, depending on the vibration frequency). In trains and road vehicles it is known that noise and pressure pulsations generated by open windows or sunroofs, at certain velocities, can create disease or disturb the passenger.

The distinction between the above two classes of phenomena is merely related to the range of frequencies implied and by the mechanism involved, but they are in principle of the same nature.

FIVs are at relatively low frequencies (typically below 100 Hz) and are induced by vortexes excited because of flow boundary layer collapse or separation at bounding walls discontinuities, such as pipe section increases or Tee junctions. When the vortexes frequencies match longitudinal acoustic modes of the piping or Helmholtz cavities modes of connected vessels relatively high shaking forces can be generated at the bends of the flow path (i.e. the fluid ducts). These shaking forces can finally excite structural bending modes, when their frequencies are close enough tot the ranges of the former. Due to the low frequencies these phenomena are not localised only around the generating source but can propagate both upstream and downstream the flow direction, in subsonic flow conditions.

The following figures show some examples of vortex sources (Fig. 2 to Fig. 7).

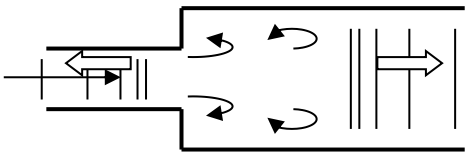

Fig. 2 - Turbulent vortex generation due to abrupt pipe diameter change (thick arrows show acoustic wave propagation).

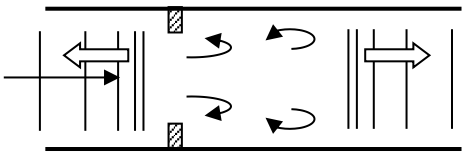

Fig. 3 - Turbulent vortex generation due to orifices or reduced bore valves (thick arrows show acoustic wave propagation).

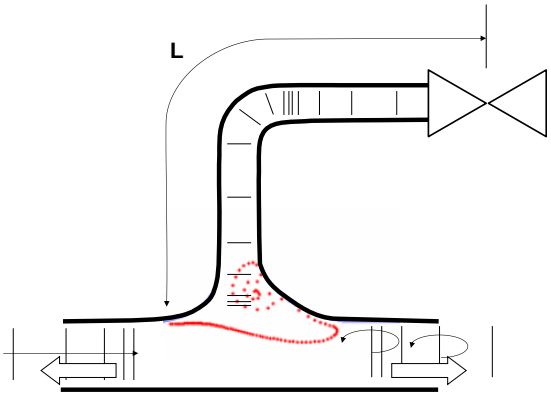

Fig. 4 - Dead branch source: Turbulent vortex generation at T-junction between a main pipe and a dead side branch (thick arrows show acoustic wave propagation).

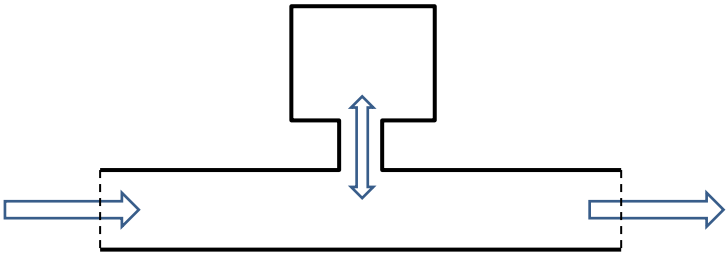

Fig. 5 - Dead cavity source: Turbulent vortex generation at T-junction between a main pipe and a dead cavity volume (vortexes at the Tee are not shown).

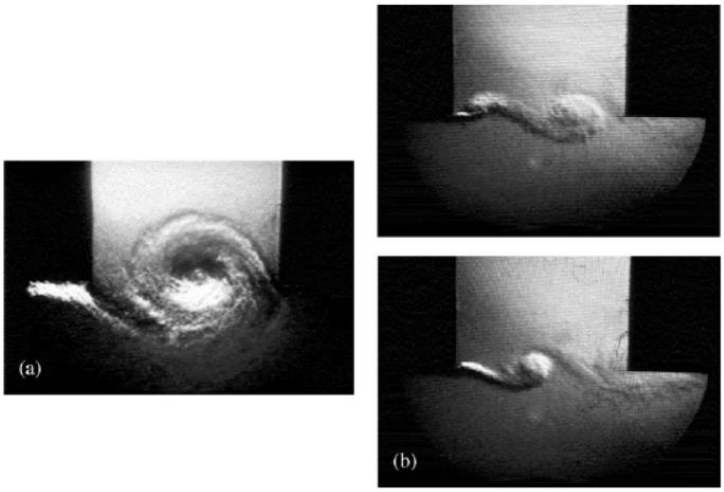

Fig. 6 - Flow visualization in a cross-junction: (a) first hydrodynamic mode; (b) second hydrodynamic mode (two successive pictures of the vortices) [Ref. 3.6.11].

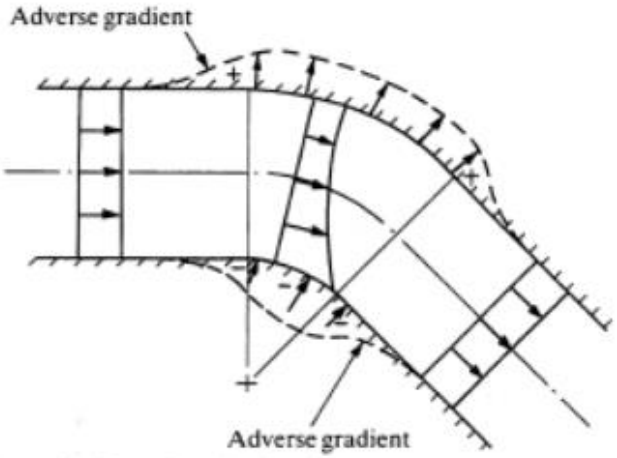

Fig. 5.31. Ideal flow through a bend

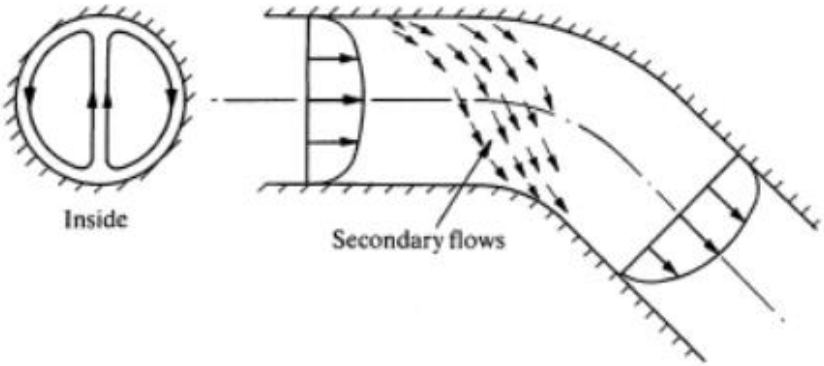

Fig. 5.32. Secondary flows

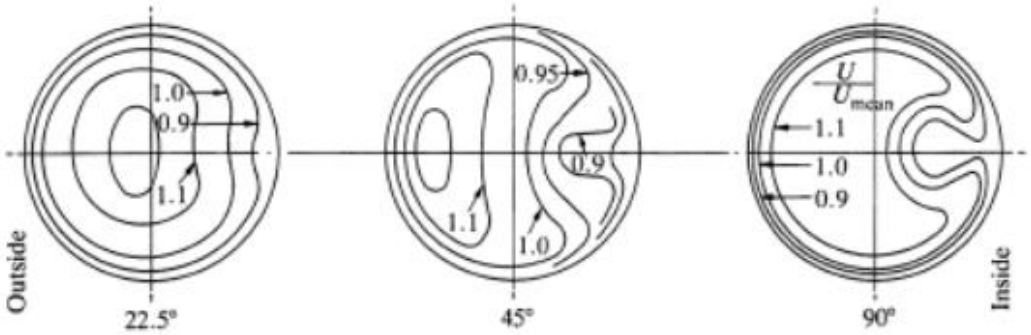

Fig. 5.33. Bend outlet velocity contours (local/mean velocity ratios)

Fig. 7 – Secondary flows at pipe bends originating downstream vortexes [Ref. 3.6.4].

AIV are at relatively higher frequencies (typically 500 to 2000 Hz); they are also induced by fluid/acoustic/structural coupling, but involving transverse acoustic and vibration modes, such as radial type acoustic modes (Fig. 8), the ring or hoop type deformation of the containing walls and the membrane modes of the containing structure (pipe or vessels). Due to the higher frequencies and the transverse modes these phenomena are usually damped in the space dimension compared to FIV, i.e. do not propagate and are localised around the source, such as high expansion ratio valves or orifices that generate vortexes at high frequency. Instead, unlike FIV, AIV can generate high and harmful noise in the surrounding environment, caused by the pipe vibrations.

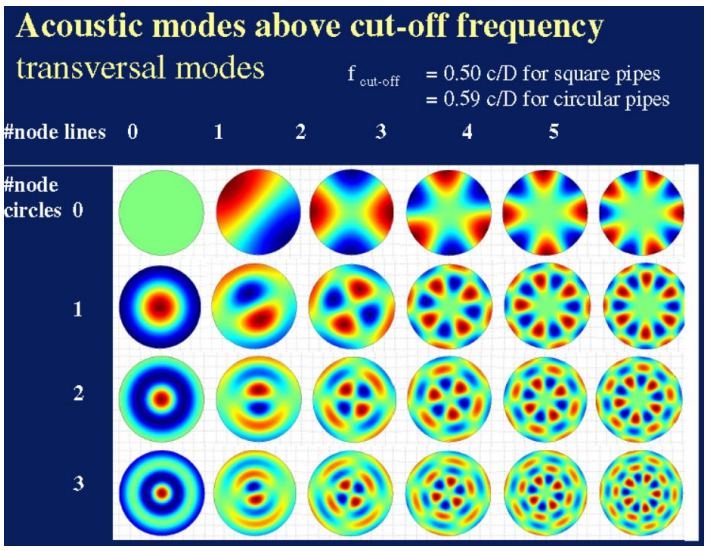

Fig. 8 – Acoustic mode patterns involved in AIVs in a pipe. These modes can excite ring vibration modes of the pipe, if frequencies match [Ref. 3.6.15].

4.2 Vortex induced by abrupt diameter increase along the flow direction

This category includes the examples shown in Fig. 2 and Fig. 3.

The vortexes frequencies range around a peak energy value corresponding to a Strouhal number normally close to 0.2[1]:

Eq. 1 $$f_s = St\frac{v}{D}$$

where:

f_s	centre frequency of the vortex turbulence [Hz]
St	Strouhal number at the centre frequency, equal to 0.2 in this case
v	average flow velocity at the throat section considered [m/s]
D	reference diameter of the vortex inducing element (e.g. orifice or minimum equivalent obstruction cross section diameter) [m]

[1] Obstruction details can modify slightly the St value for maximum vortex excitation. The value of 0.2 applies in the most common cases.

It is commonly accepted that the energy distribution of the Strouhal vortex turbulence decreases by a slope of ± 3 dB/octave symmetrically around the above centre frequency value (Fig. 9).

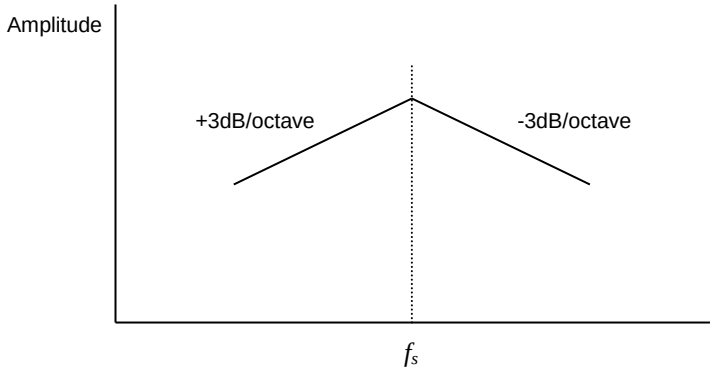

Fig. 9 - Energy distribution of the Strouhal vortex turbulence across the centre frequency.

The above frequency spread implies that a resonance may arise also near, yet not in coincidence with the centre frequency as function of the dynamic acoustic characteristic of the fluid system in the zone of the generating obstruction, or in more correct terms, as function of the impedance seen by the source (Fig. 10). This is referred also as “acoustic lock-on”.

A correct analysis shall then focus on verifying that any vortex source by obstructions has a centre frequency at a suitable distance from natural acoustic frequencies of the piping, by a transfer function analysis. Then a check shall also be made as to the distance between the latter, i.e. the acoustic lock-on frequency, and the structural natural frequencies of the piping.

The standard criterion is to ensure at least 20% frequency separation margin [Ref. 3.6.16/18].

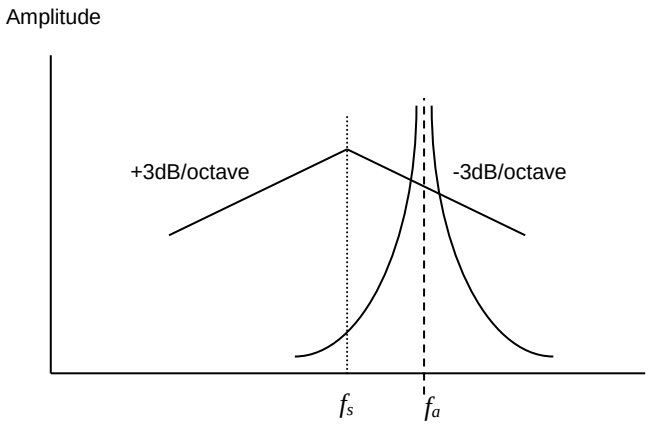

Fig. 10 - Possible resonance aside the turbulence Strouhal centre frequency.

4.3 Vortex induced at pipe branches and Helmholtz resonators

This category is exemplified in Fig. 4 and Fig. 5 and visualised in Fig. 6. It applies to all fluid path branches created by isolation valves, by-pass lines or spare lines, in plants, or by enclosures able to trap the fluid while maintaining it in physical continuity with the flowing one along a main path.

In this case acoustic lock-on can occur also with vortex sources different from those at the Tee of the branch of concern, i.e. at upstream or downstream obstructions or Tees, should the respective frequencies match.

The acoustic response to be considered against the vortex matching is that of a relatively broad system, extending beyond the immediate surroundings of the vortex source, above all if this latter is prone to excite low frequencies that are associated to large standing wave lengths that can reach parts of the system or combinations of pipe elements that, by themselves, would not resonate at the frequency of the disturbance, e.g. because are too short.

The worse conditions for side branches or cavities occur when they do not convey any flow (dead branches). Indeed, the fluid flow produces a significant yet low damping of the acoustic response that disappears or is negligible at no flow conditions.

Nevertheless, significant and disturbing side branch resonances may occur even in flowing conditions along the branches affected that, in this case exchange with the main line not only an oscillating fluid but also a net flow rate.

4.4 Vortex induced at pipe bends

The flow downstream pipe bends is characterised by vortexes generated by the different centrifugal forces acting on the inner and outer side streamlines when passing through the curved pipe (Fig. 7).

Dean (1927), was the first to identify and analyse these flow patterns, which, by themselves may be associated to non-periodic pulsations, such as in laminar flow conditions (Fig. 11).

In turbulent flow conditions, instead, the vortexes flow pattern downstream the bend is very complex and characterised by so called switching modes of the two Dean vortexes that periodically prevail at any downstream sections (Fig. 12).

The flow pulsations associated to these vortex patterns are very complex, not yet completely understood as of today and simulated with insufficient accuracies by CFD models [Ref. 3.6.19]. For the purpose of this study, the main parameter of relevance, as regards the generation of resonant self-excited acoustic response, is the vortexes “switching” frequency. This is defined again by the Strouhal number (Eq. 1), which in this case is very low and is reported in the order of 0.002. Other frequency components, at higher values of St, have much lower intensity [Ref. 3.6.19].

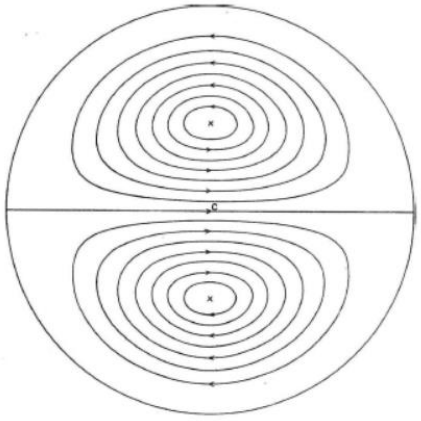

Fig. 11 – Theoretical “Dean” vortexes, downstream bends [Ref. 3.6.19].

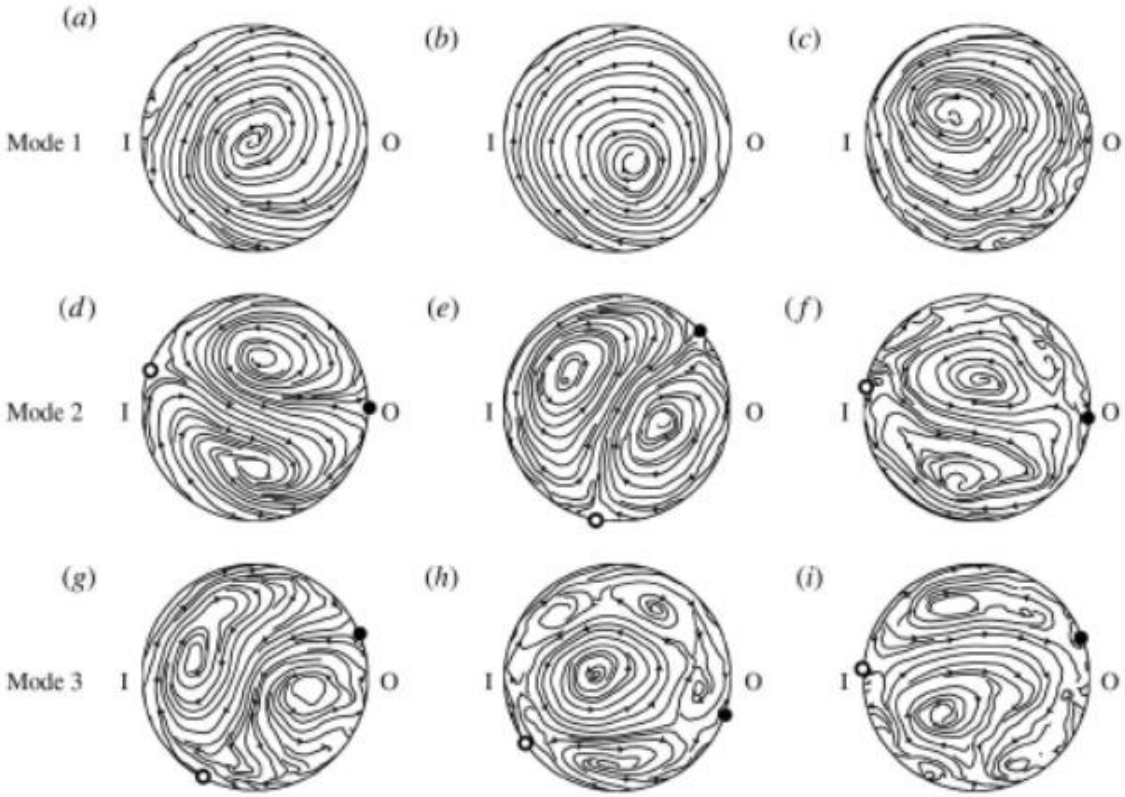

Fig. 12 – First three POD modes for Re = 2.5×10^4, (a, d, g) 5D, (b, e, h) 12D and (c, f, i) 18D; (a-c) Mode 1, (d-f) Mode 2 and (g-i) Mode 3. The inner and outer stagnation point is indicated with open and filler circles, respectively [Ref. 3.6.19].

4.5 Relevance for the n-Tof Target # 3 project

A breakdown of the n-Tof target #3 with the main nomenclature is shown in Fig. 13, while the main coolant flow paths are shown in Fig. 14.

The analysis performed in this study regards the flow conditions between the entry port to the cradle (lower framed detail in Fig. 14) and the top of the anti-creep plates channels (upper framed detail in Fig. 14).

Out of the two subclasses, abrupt section changes and side branches, the latter are most relevant for the n-Tof because the flow entering the cradle is passing in front of the small openings.

The potential vortexes sources along the cooling fluid paths are the circular arcs (≈ 142 mm long) through which the gas passes from the bottom ducts into the channels between the anti-creep plates. The flow streams are disturbed by the 90° bend of the feed pipes just upstream the respective inlet into the cradle.

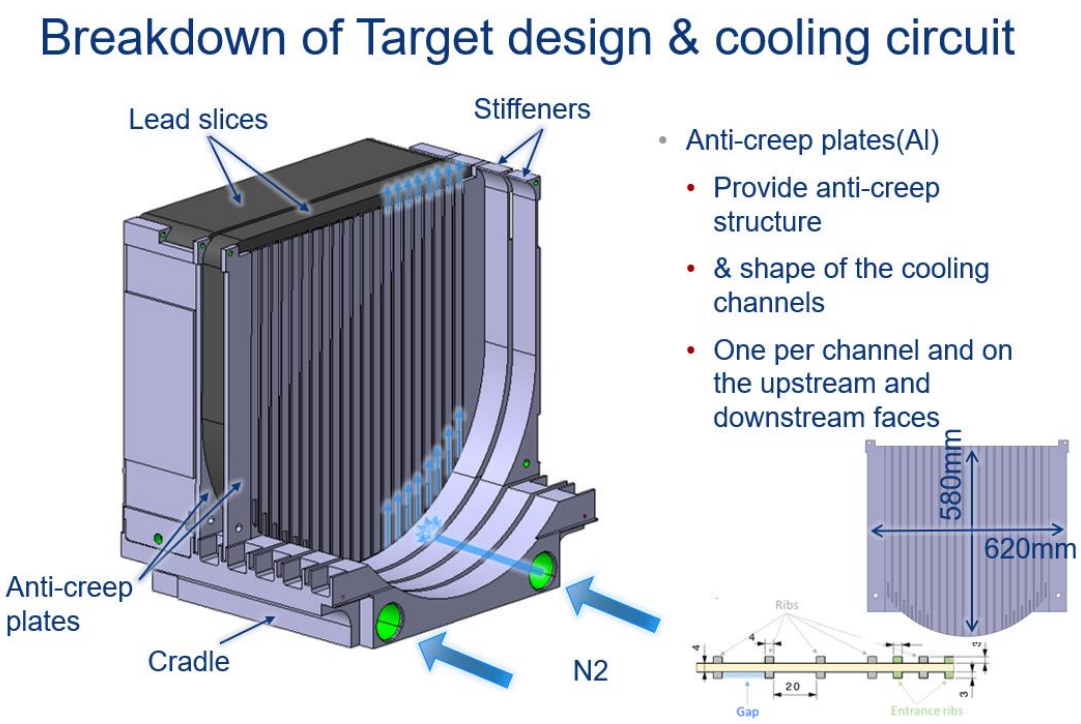

Fig. 13 – n-Tof Target #3 breakdown of design and cooling circuit [Ref. 3.3.1].

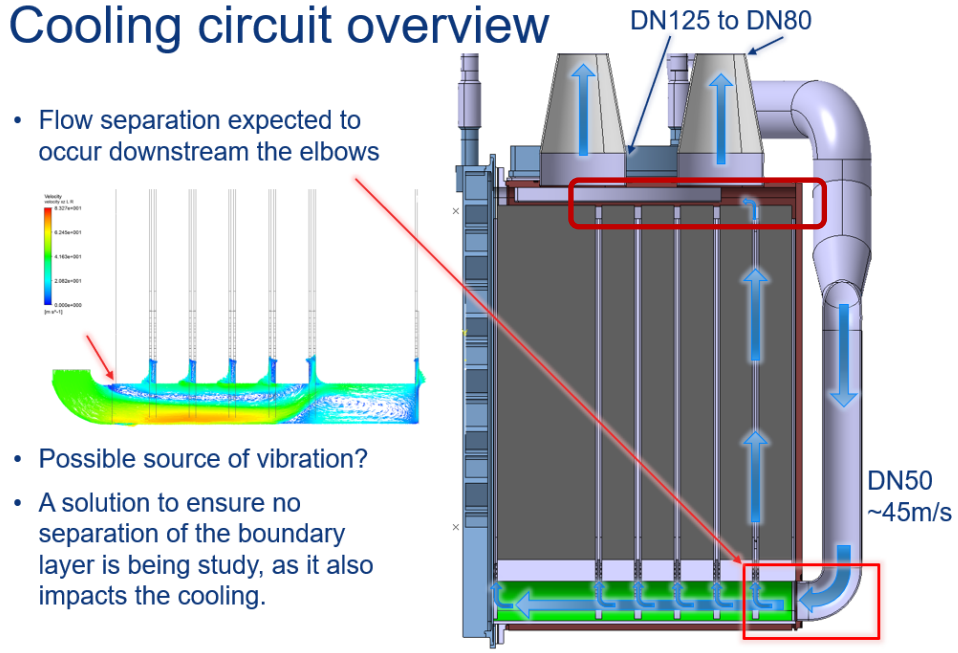

Fig. 14 – n-Tof main flow paths [Ref. 3.3.1].

The vortexes generated downstream these entry bends have a very low center frequency that can be calculated by the local Strouhal number, according to Eq. 1 and the value reported for 90° bends [Ref. 3.6.19[2]].

Eq. 2 $$f_s \cong 0.002 \frac{45}{50 \cdot 10^{-3}} = 0.18\ Hz$$

This frequency is of such a low order of magnitude as not to imply FIV in the cooling channels of the n-Tof Target # 3.

The n-Tof target #3 gas flow occurs at relatively low expansion ratios along the fluid path, thus only the FIV category is of concern, according to the above customary distinction. However, the small dimensions of this component and of the fluid channels imply relatively high frequencies, bridging the above mentioned FIV-AIV rough ranges even considering the cavity and longitudinal type acoustic resonances.

4.6 Relevant bibliography for the study of FIV for the n-Tof Target #3

Rev. 1

4.6.1 Introduction

This section provides a brief overview of the main literature works that pave the way to the FIV analysis of side cavities and pipe branches, of relevance for the present study.

These works relate mostly to the process industry (gas compressors, pumps and turbines) or the automotive industry. Earlier works were more general and related also to musical instruments, such as flute and organ pipes, which behave based on the same physics.

The works reported are cited in chronological order.

4.6.2 Junkowski W.M., Botros K.K., Studzinski W [Ref. 3.6.3]

The work by these authors is among the fundamental references in the FIV literature, even if it dates back to 1988, because it reports important experimental data on various dead pipe branches and reflective end conditions over a wide range of Reynolds number (1×10^5 to 16×10^6) and with usual values of the Mach number in correctly sized gas plants piping (0 to 0.2). This work was also cited in subsequent works by several authors.

This work explained also the mechanism of the onset and stabilization of the self-excited pulsations, formulating empirical dimensionless expressions to predict the frequency and amplitude of the pressure pulsations at the most responsive points of dead branches, in connection with an earlier work by Howe, who had suggested a physical mathematical approach to calculate the power generated by the vortical flow [Ref. 3.6.1/2].

The authors developed a simple equivalent model of tone source, based on a hypothetical oscillatory piston and two transfer matrices. The data collected in the experiments and the source model allowed defining a procedure to estimate the tone frequency and its amplitude for complex systems with side branches subject to the applicability of the acoustic plane wave propagation theory.

The expressions proposed, for the Strouhal number at which the maximum tone amplitude appears and for the maximum pressure pulsation amplitude, were extracted by dimensional

[2] The Strouhal number reported is relevant to experiments made at lower values of the Reynolds number (up to $2.2\text{x}10^5$), which covers the operational range of the n-Tof Target #3.

analysis and correlations and remained in the 2008 Energy Institute Guidelines, that considered the regression tolerance for upward coefficient corrections [Ref. 3.6.16].

Eq. 3 $$St_m = 0.399\left(1 - {r_c}/{d_{c,eq}}\right)^{0.622}\left({d_{c,eq}}/{D_p}\right)^{0.316} M^{-0.083}\left({Re}/{10^6}\right)^{-0.065}$$

The resulting average deviation of the above formula is ±5.35%[3].

4.6.3 Bruggeman J.C. et al. [Ref. 3.6.6]

This paper is another of the first literature pillars for those who study FIVs at Tee junctions and, in general, to understand the self-excitation mechanism, particularly at high Reynolds number.

This work analysed, in theory and experiment, the behaviour of a sequence of two side branches, of variable length at various Reynolds and Mach numbers.

The authors found that at high pulsation values, at which friction becomes negligible compared to acoustic radiation losses through the main flow stream, the pulsations (in particular the maximum values at the end of dead branches) scale with $\rho c_s U_o$ and not with $½\rho U_o^2$, as thought before, and that are independent of Mach number and of the length/diameter ratio of the side branches. They instead depend on the piping geometry.

The authors defined three level classes of pulsations to distinguish the phenomena:

Low amplitude level: $$\frac{p'}{\rho c_s U_0} \leq 10^{-3}$$

Moderate amplitude level: $$10^{-3} \leq \frac{p'}{\rho c_s U_0} \leq 10^{-1}$$

High amplitude level: $$\frac{p'}{\rho c_s U_0} \geq 10^{-1}$$

noting that $$\frac{p'}{\rho c_s U_0} = \frac{M}{2}\frac{p'}{{1}/{2}\rho U_0^2}$$

Another result of the experimental part of this work, which allows sharing data from experiments and models developed either with squared or circular pipe sections and considering the rounding of the upstream edge, consists in the following equivalence relations to be used in the Strouhal number definition and to mutually convert data for circular sections or squared sections.

Eq. 4 $$L_c = \frac{\pi}{4} d$$

and

Eq. 5 $$d_{eq} = d + r_c$$

Where L_c, d and r_c are respectively the equivalent square section side (i.e. the average width of the cavity opening along the main flow direction), the cavity opening diameter, if circular and the radius of curvature of the upstream edge (if squared) or of the Tee branch (if circular).

[3] Note that the Energy Institute Guidelines (Ref. 3.6.16), report the same formula where the coefficient 0.399 is multiplied by the upper uncertainty margin factor, i.e. 0.399 x (1+0.0535) = 0.420.

This experimental work found also that the rounding of the cavity edge, a part from its influence on the S_t value, makes the amplitude of the pulsations higher than sharp edges[4].

4.6.4 Rogers L.E. [Ref. 3.6.7]

This author applied the previous works by Junkowski & others and Bruggeman & others above cited to analyse pulsation problems in a large gas compression facility. Having collected data at higher Reynolds number than Junkowski, he found that the Strouhal number is relatively independent from M and Re for Re > 16x10^6, thus he proposed a simplification of Eq. 3 for this high range:

Eq. 6 $$St = 0.413 \left({d_{c,eq}}/{D_p} \right)^{0.316}$$ (for Re > 16x10^6)

The resulting average deviation of the above formula is ±13%. This relation also remained in the recommendations by the Energy Institute [Ref. 3.6.16][5].

4.6.5 Ziada S., Shine S. [Ref. 3.6.9]

These authors studied experimentally and synthesized by design charts a variety of single and pairs of closed side branches in both tandem and cross configuration.

As an original part of their work they introduced, moreover, the study of the effects of a 90° elbow upstream the side branches, analysing the sensitivity of its distance from the first side branch on the Strouhal number at which acoustic modes are excited to the maximum pressure pulsation level.

The results show that when the branch is at the outer side of the elbow (curve 1 in Fig. 15) the local velocity is higher than the average velocity.

The resonance therefore starts at a lower flow rate, i.e., at a higher Strouhal, referred to the average velocity. Moreover, the relative amplitude becomes higher than the case of uniform flow (curve 3 in Fig. 15). This increase, however, is rather superficial because the relative amplitude is based on the average velocity, which is lower than the local velocity at the mouth of the branch, which excites the resonance. Conversely, when the branch is at the inner side of the elbow (curve 2 in Fig. 15), the onset of resonance is delayed, i.e., it occurs at a higher flow rate, and the relative amplitude becomes (superficially) smaller. The three curves shown in Fig. 15 may well become very close to each other if the local flow velocity is used to calculate the Strouhal number and the relative amplitude.

They also showed that tandem and coaxial (cross like) branches show much higher pressure pulsation amplitudes than single branches at same flow conditions.

The resulting Strouhal number at which maximum pulsations occur extends over a wide range (0.35 to 0.62), being also dependent on the diameter ratio between the side branch and the main line.

---

[4] This result was found later, by other authors, not to be general as in multiple branches or in flowing pipes the influence is opposite.

[5] Note that the Energy Institute Guidelines (Ref. 3.6.16), report the same formula where the coefficient 0.399 is multiplied by the upper uncertainty margin factor, i.e. 0.413 x (1+0.13) = 0.467.

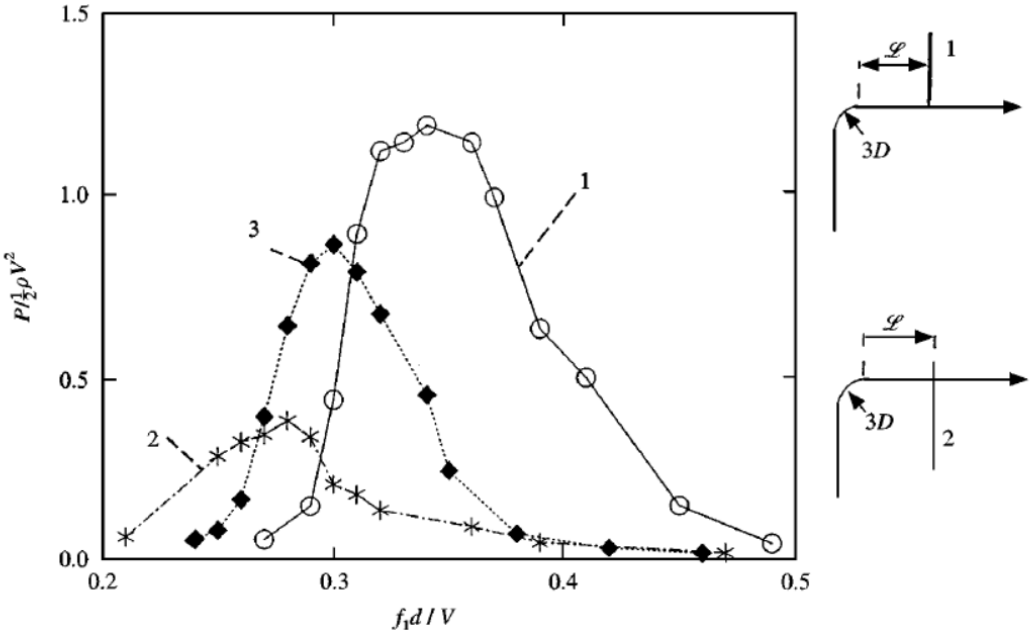

Fig. 15 – Effect of the upstream elbow on the acoustic response of a single branch; o, branch at the outer side of the elbow; *, at the inner side; ♦, no elbow. d/D=0.135, f_1 = 490 Hz, $\mathscr{S}/D$ = 1.85, Ps = 3 bar. [reported from Ref. 3.6.9].

The authors also confirmed the equivalence between rectangular and circular side branch data to use their correction charts for 90° elbows with rectangular section branches providing that the Strouhal number is calculated according to the equivalent diameter proposed by Bruggeman:

Eq. 7 $$d_{c,eq} = \frac{4}{\pi} L_c$$

Furthermore, they confirmed the addition of the upstream edge radius r_c to the former in the Strouhal number calculation or derived quantities thereof.

4.6.6 Peters M., van Bokhorst E. [Ref. 3.6.10]

These authors extended the study of side branches, formerly limited to dead side branches (i.e. with no flow condition) with the main flow going through the straight pipe, to flowing side branches by a variety of branching configurations and Tee edges rounding radii.

The results discussed show sensible variations of the Strouhal number at which the maximum amplitude occurs, as well as wide variations of the latter as function of the branching geometry, the main flow scheme and the upstream and downstream edges radius values. The overall range reported shows maximum pulsation amplitudes with St from 0.2 up to 0.4.

This study was supported by both numerical analysis (vortex blob model method) and experiments with pipe diameter of 42 mm.

4.6.7 Hemon P., Santi F., Amandolèse X. [Ref. 3.6.12]

This work deals with a model and an experimental verification of the resonance of an Helmholtz cavity aimed at solving disturbing pulsations and disease to automobiles passengers with sunroof opening.

Despite the different field of application, the results are interesting as regards the Helmholtz parameters, in particular the extended (or added) neck length parameterization to account for the stream tube elongation inside the cavity and the consequent inertia that lowers the actual Helmholtz resonance compared to the theoretical one based on the geometrical length H_c.

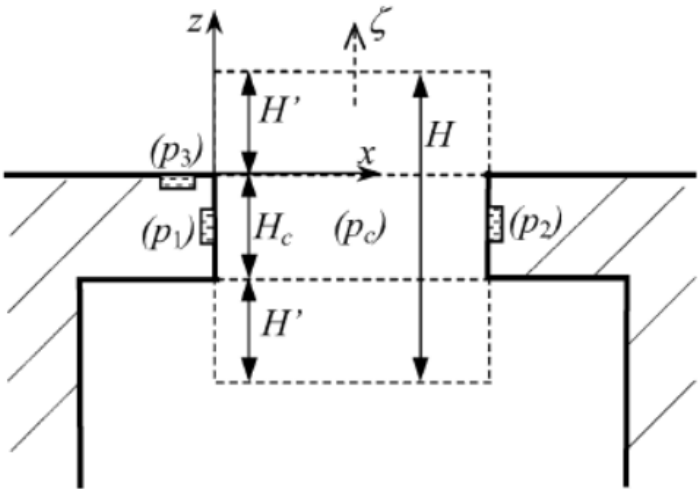

Fig. 16 – Helmholtz cavity nomenclature in Ref. 3.6.12].

The authors report from previous sources the following relation that has been also used in this study (the symbols applied are those used in the calculation sheets according to the symbols list in sec. 3.2).

Eq. 8 $$H_a = 0.85 \frac{A_c^{0.75}}{\sqrt{l_{cp}}} \qquad (6)$$

Thus the total actual length of the Helmholtz resonator neck is:

Eq. 9 $$H = H_c + 2 \cdot H_a$$

Rev. 1

and the Helmholtz resonance frequency is then:

Eq. 10 $$f_H = \frac{c_S}{2\pi}\sqrt{\frac{A_C}{V_C H}}$$

4.6.8 Amandolèse X., Hemon P., Santi F. [Ref. 3.6.13]

In this work the authors of the preceding paper extended the experimental work to develop a model of the resonator and verify attenuation methods of the disturbing noise.

6 Note that H_a corresponds to H' in Fig. 16.

The data reported are interesting as they refer to elongated rectangular openings of the grazing flow towards the Helmholtz cavity, which is similar to the conditions of the nTof Target #3 first acoustic mode conditions.

The Strouhal number of the reported experiments (Fig. 17) are also a useful reference that fits the calculations of this study, based on independent formulations, as will be shown in the following sections.

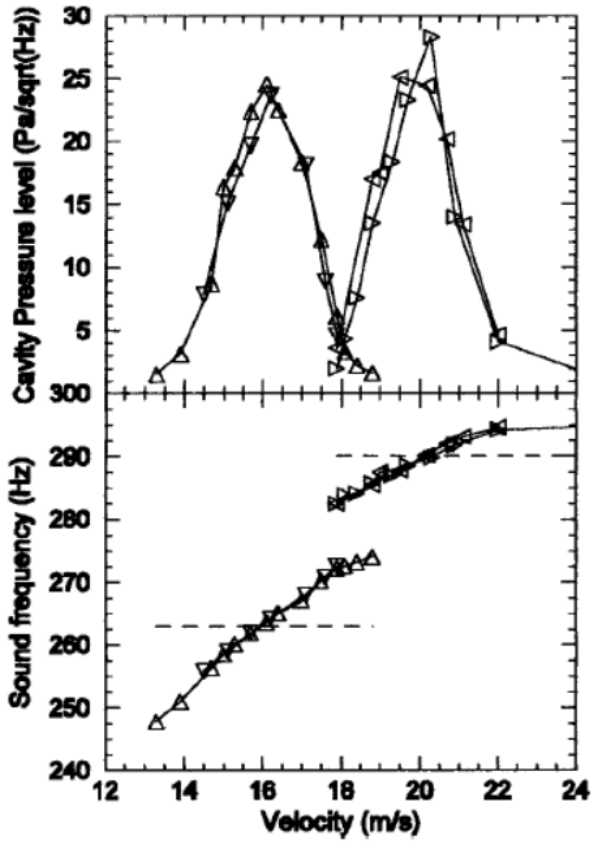

Fig. 17 – Cavity pressure level and corresponding frequency vs. U_0 for a deep cavity [reported from Ref. 3.6.13]. Note: the peaks at 16 and 20 m/s correspond to St = 0.329 and 0.290 respectively, for the rectangular test cavity of 20 mm neck width along the flow direction.

4.6.9 Ziada S., Scott S., Arthurs D. [Ref. 3.6.14]

This work is similar to that by Peters & van Bokhorst recalled in sec. 4.6.6, but they focus on the effects of combining and dividing flows at Tee junctions, while the former work was limited to flowing conditions but with a single flow stream, either through the main pipe or to/from this from/to the side branch.

The interesting result is that converging flows are able to generate higher pulsation levels than diverging flows and that the former have the maximum for Strouhal number around 0.5, while the latter have the maximum for Strouhal around 0.2 (Fig. 18).

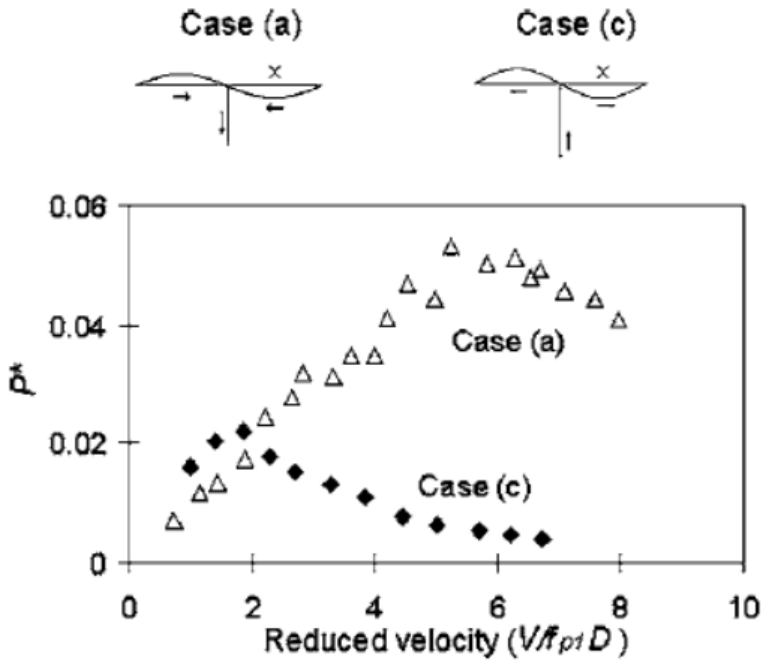

Fig. 18 – Normalized amplitude of the primary mode $P^*(f_{p1})$ for cases (a) and (c) as a function of the reduced velocity based on the primary mode frequency f_{p1} [reported from Ref. 3.6.14]. Note: note that the reduced velocity = $1/St$, thus the peaks at 2 and 5.2 correspond to St = 0.5 and 0.19 respectively.

4.6.10 Energy Institute, [Ref. 3.6.16]

In 1999 the Marine Technology Directorate (MTD) in the UK published Guidelines for Avoidance of Vibration Induced Fatigue in Process Pipework. In 2008, the Energy Institute in the UK revised and reissued these guidelines.

These cannot be used as design tools but just as screening tools to precede a deeper design or verification analysis.

In any case, they confirm the formulation above reported by Jounkowski & others in sec. 4.6.2, and the settling formulation by Rogers, reported in sec. 4.6.4 for high Reynolds number (i.e. grater than $16x10^6$), for the prediction of the critical flow conditions and frequencies in fluid processing pipes.

5 BASE DATA

5.1 Operating conditions

The operating conditions used as reference for the calculations, based on the data provided by the Client, are the following:

Cooling gas pressure at cradle inlet		1.013 ± 0.1	bar a
Cooling gas temperature at cradle inlet		20	°C
Cooling gas mass flow rate (two cradle tubes)			
	case A	787	Nm^3/h
	case B	1005	Nm^3/h
Cooling gas mass flow rate (one cradle tube: 50% of total)			
	case A	0.137	kg/s
	case B	0.174	kg/s
Gas	Nitrogen	100%	

5.2 Fluid properties

The gas properties of interest for the analysis performed are shown in Table 1. They have been calculated by the REFPROP software programme of the NIST [Ref. 3.6.20]

Temperature	T	20.0	[°C]
Pressure	p	1.013	[bar a]
Molar mass	μ	28.0135	[kg/kmole]
Compr. factor	z	0.99976	--
Density	ρ	1.1645	$[kg/m^3]$
Absolute viscosity	η	$1.76\ 10^{-5}$	[Pa s]
Kinematic viscosity	ν	$1.51\ 10^{-5}$	$[m^2/s]$
Specific heat ratio	γ	1.4014	[--]
Speed of sound	c_s	349.1	[m/s]

Table 1 – Reference gas properties at the operating conditions [Ref. 3.6.20].

The gas properties at the sensitivity conditions (± 0.1 bar from the base case) are not reported for brevity. They are part of the detailed calculation report under Annex A1.

5.3 N-Tof data

Flow vortexes can be excited at the side opening of the cavities facing the gas flow through the main tube of the n-Tof Target cradle.

In the present case the main duct is one of the nitrogen lines feeding the cooling flow at the bottom of the anti-creep plates cradle, while the side cavity consists of each of the five volumes trapped between two anti-creep plates of the Target block (see Fig. 19 and Fig. 20).

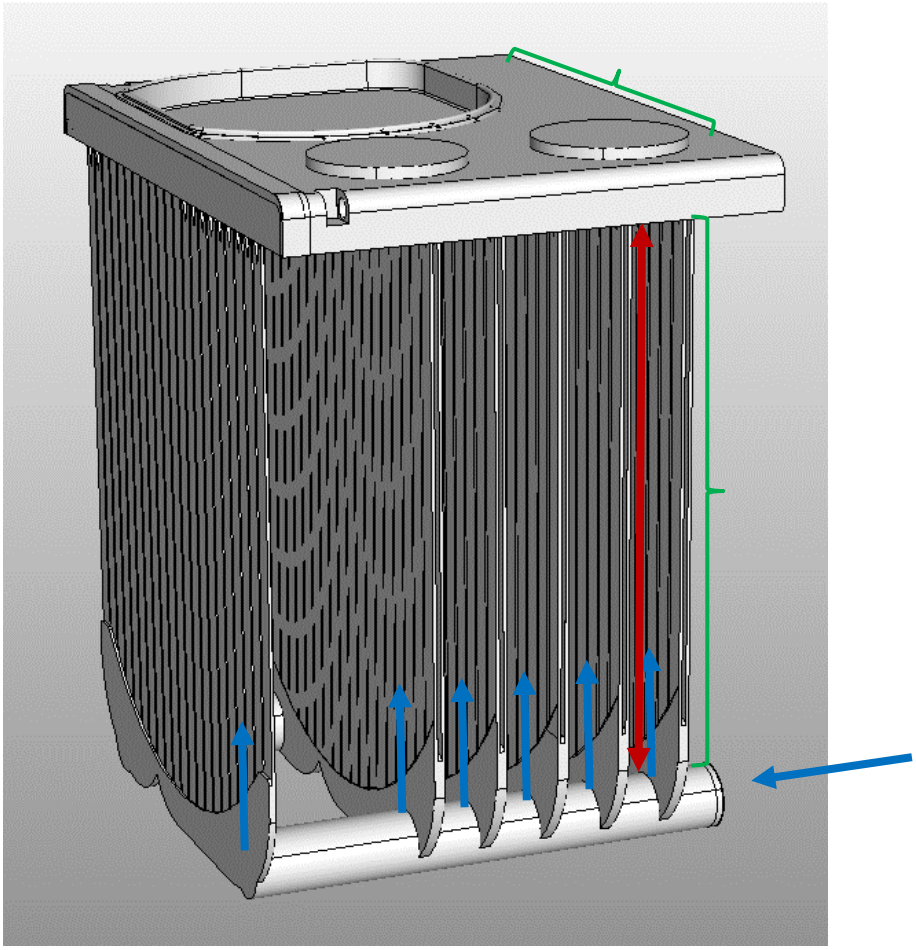

Fig. 19 – Nitrogen wet volume and parts of the n-Tof Target # 3 [Ref. 3.4.4].

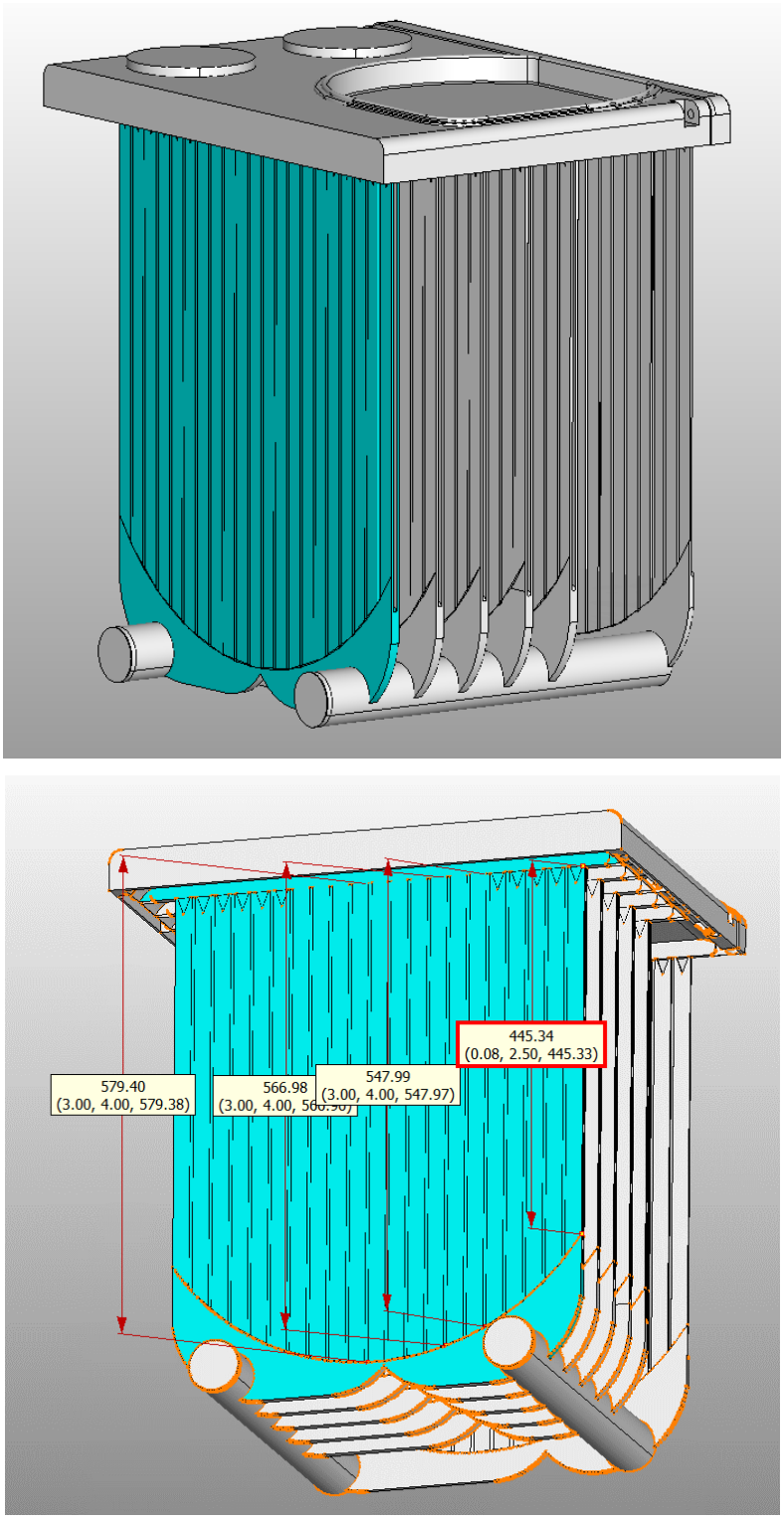

Fig. 20 – Helmholtz cavity of the first acoustic mode (one out of the five subject to grazing flow at the bottom neck port) and length of the channels [Ref. 3.4.4].

The geometrical data used for the calculations are summarised in Table 2, where the base data are referred to the figures and the derived quantities are shown with their calculation equations.

Header pipe inner diameter (Fig. 24)	D_p	60.3	[mm]
Anti-creep plate channels length (average along flow, Fig. 20)	L_{ap}	550.0	[mm]
Anti-creep plate channels gap (between ribs, Fig. 22)	b_{ap}	20.0	[mm]
Anti-creep plate channels thickness (across flow, Fig. 22)	t_{ap}	3.0	[mm]
Number of channels per Anti-creep plate, Fig. 20)	n_{ap}	42.0	[--]
Anti-creep plate cavity plenum volume (approx., Fig. 24)	V_{pl}	367884	[mm^3]
Anti-creep plate cavity total volume ($V_c = n_{ap} * L_{ap} * b_{ap} * t_{ap} + V_{pl}$)	V_c	1753884	[mm^3]
Cavity width (along cradle header pipe flow, Fig. 22)	L_c	10.0	[mm]
Cavity equivalent diameter, for $f_v(St)$ calc. (Eq. 7: $d_{c,eq} = \frac{4}{\pi} L_c$)	$d_{c,eq}$	12.7	[mm]
Cavity breadth at the cradle header pipe ports ($b_c = ¾ * \pi * D_p$)	b_c	142.1	[mm]
Cavity edge radius (sharp edge assumption due to cutting)	r_c	0.0	[mm]
Cavity neck section area ($A_c = b_c * L_c$)	A_c	1421	[mm^2]
Cavity neck perimeter ($l_{cp} = 2 * (b_c + L_c)$)	l_{cp}	304	[mm]
Cavity neck thickness (Cradle header pipe thickness, estim.)	H_c	3.5	[mm]
Cavity neck added thickness (Eq. 8: $H_a = 0.85 \frac{A_c^{0.75}}{\sqrt{l_{cp}}}$)	H_a	11.3	[mm]

Table 2 – Geometrical data used for the calculations of the vortex and acoustic frequencies.

6 VORTEX SOURCES DEFINITION AND FREQUENCY CALCULATIONS

6.1 Sources

The potential vortexes sources considered are the circular arcs (≈ 142 mm long) through which the gas passes from the bottom ducts into the channels between the anti-creep plates. These openings have a small dimension (10 mm) along the fluid direction. Its dimensions are to be considered in the calculation of the Strouhal number that shall then be compared with literature data on closed or flowing side branches (see sec. 4.6).

The main flow velocity in front of the openings is calculated for each one considering 50% of the total flow rate entering each of the two ducts and decreased by 1/5 after the passing in front of each of the anti-creep plate ports.

The reduction of the local velocity in front of the ports, due to the 90° bend upstream the ducts inlet is neglected, considering that a wide range of Strouhal number values, between 0.2 and 0.5, is considered for the acoustic lock-on checks. This assumption is anyway conservative as the vortex sources are on the inner side of the bend, thus in a lower velocity zone (4.6.5).

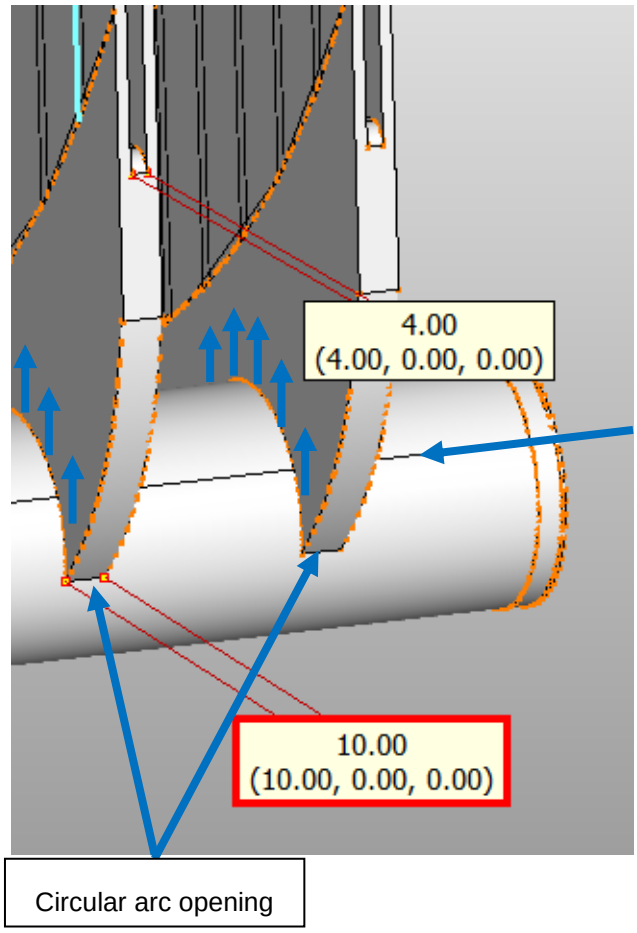

Fig. 21 – Detail of the side opening along the cradle tube [Ref. 3.4.4].

As already mentioned in sec. 4.4 the vortexes induced at the 90° inlet bend would be at too low frequency to develop a pulsating pattern, both because they are associated to very low Strouhal numbers but also because they would need a much longer cradle straight pipe downstream the bend to fully develop a tonal pulsating nature.

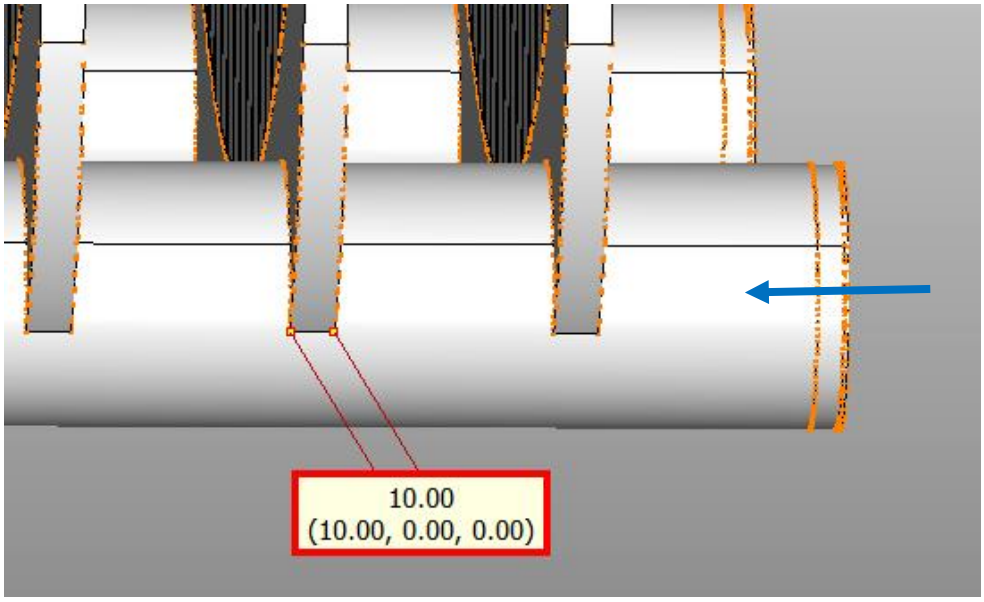

Fig. 22 – Details of the cavities edges and acoustic path considered [Ref. 3.4.4].

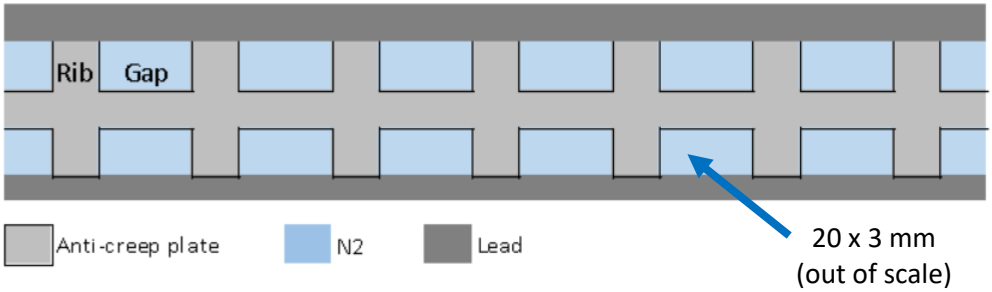

Fig. 23 – Nitrogen wet parts considered for the Helmholtz cavity volume calculation (all the 21 x 2 channels are considered) [Ref. 3.4.4].

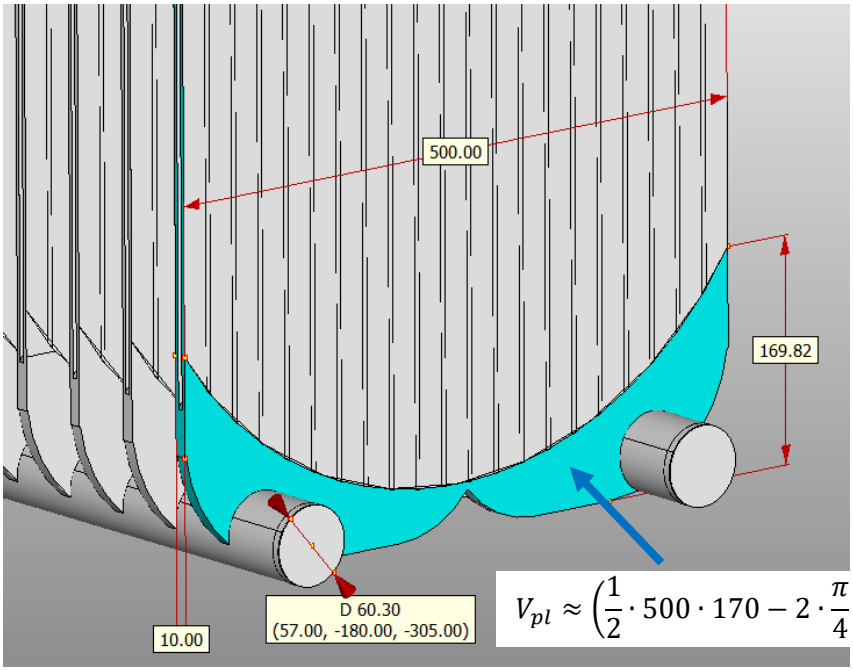

Fig. 24 – Gas channels distribution plenum (highlighted in cyan) [Ref. 3.4.4].

6.2 Frequencies calculation

The above geometries, operating data and those calculated thereof have been used to calculate the vortex frequencies at which self-excited acoustic mode could lock-on if in tune.

The minimum and maximum Strouhal number assumed as a conservative range for the definition of the possible lock-on conditions are respectively St_{min} = 0.2 and St_{max} = 0.5, as already mentioned.

Table 3 shows the equations and their application to the first side opening, subject to the whole flow coming from the cradle inlet tube, i.e. 50% of the total cooling gas flow, under the operating condition A.

In annex A1 the calculations are reported for each side opening with gradually reduced flow rate for both operating condition and for the sensitivity upper and lower pressures.

Fig. 25 shows the range of variation of the mean gas velocity at opening inlet that has to be considered for the various ports and operating conditions, on one cradle distribution tube.

The variation of the resulting vortexes frequencies are reported in sec. 9.

Rev. 1

Mean grazing flow velocity:	$v_0 = \frac{mfr}{\rho \pi/4 \left(D_p/1000\right)^2}$	v_0	41.1	[m/s]
Reynolds number:	$Re = \frac{\rho v_0 \left(D_p/1000\right)}{\mu}$	Re	1.64 10^5	[--]
Mach number:	$Ma = \frac{v_0}{c_s}$	Ma	0.118	[--]
Low Re Strouhal number	(see Eq. 3, for Re ≤ 16 x 10^6)	St_1	0.328	[--]
High Re Strouhal number	(see Eq. 6, for Re > 16 x 10^6)	St_2	0.253	[--]
Matching Strouhal number	(=St_1 or St_2 depending on Re)	St	0.328	[--]
Central vortex frequency:	$f_{v,0} = St \frac{v_0}{(d_{c,eq}+r_c)/1000}$	$f_{v,0}$	1058	[Hz]
Min vortex frequency:	$f_{v,min} = St_{min} \frac{v_0}{(d_{c,eq}+r_c)/1000}$	$f_{v,min}$	645	[Hz]
Max vortex frequency:	$f_{v,max} = St_{max} \frac{v_0}{(d_{c,eq}+r_c)/1000}$	$f_{v,max}$	1613	[Hz]

Table 3 – Calculation of the vortex frequencies.

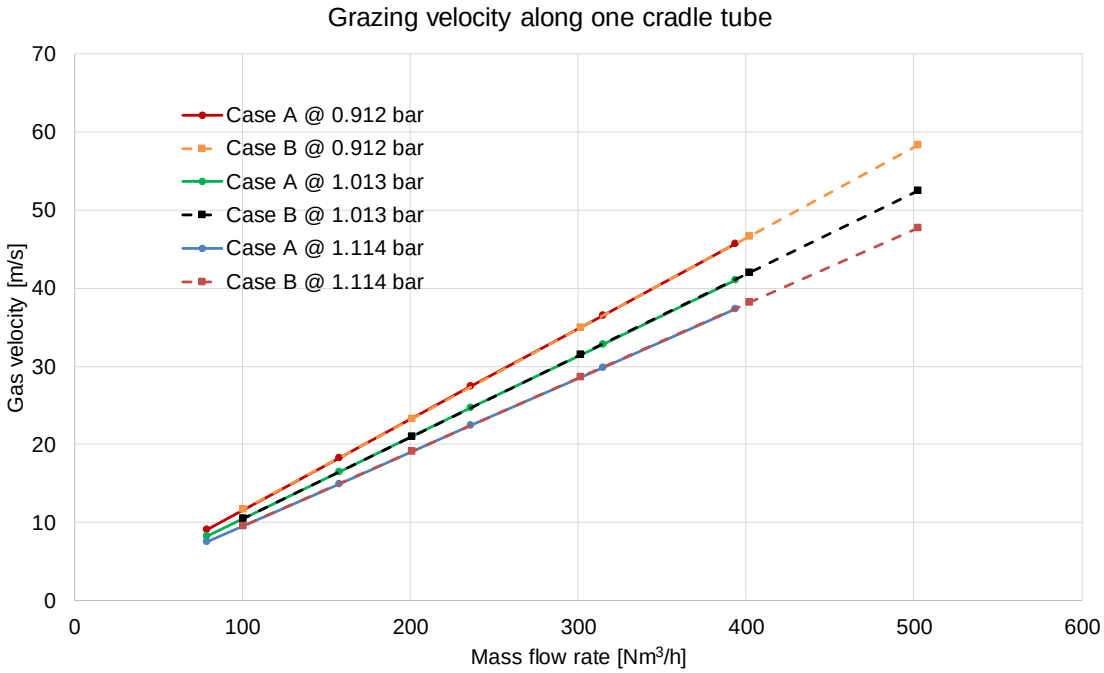

Fig. 25 – Variation of the gas velocity with the mass flow rate at the side opening (grazing).

7 ACOUSTIC FREQUENCIES CALCULATIONS

The acoustic systems considered to potentially resonate are the following.

7.1 Helmholtz type oscillator

This is composed of the volume trapped between two anti-creep plates (Fig. 20, Fig. 21 and Fig. 22), i.e. all the 21 x 2 gaps like those shown in cross section in Fig. 23, considering an average length of the channels of 550 mm, and a cross section of each channel of 3 x 20 mm (thickness x gap left between ribs).

The total volume of this cavity sums up to ≈1700 cm^3, including the distribution zone on the lower part (Fig. 24).

The Helmholtz cavity volume communicates by a potentially oscillating flow through a neck port having a width of 10 mm, a developed breadth of 142 mm along an arc of about 270° and a thickness of 3.5 mm (estimated).

An added thickness of 13.2 mm is accounted for, to consider the actual oscillating fluid stream inertia, according to Hémon, Santi, Amandolèse (see sec. 4.6.7).

The frequency of the Helmholtz mode resonance is then given by Eq. 9 and Eq. 10, yielding the values reported in Table 4, for the first side opening, subject to the whole flow coming from the cradle inlet tube, i.e. 50% of the total cooling gas flow, under the operating condition A.

Table 4 shows the margin between the resonant frequency and the central vortex frequency, i.e. that at which maximum pulsation amplitudes are expected, derived from Table 3 and the result of the check of the necessary condition for lock-on. i.e.:

- That the resonant frequency falls within the min-max vortex frequency range ±20%

  AND

- That the Reynolds number of the grazing flow is greater than the minimum to self sustain the oscillation (10^5)

Helmholtz acoustic frequency	f_H	310	[Hz]
Acoustic Margin (from Central vortex frequency)	AM_H $(center)$	-71%	[--]
Lock-on condition $(0.8 * f_{v,min} < \boldsymbol{f_H} < 1.2 * f_{v,max})$ AND $(Re > Re_{min})$	ALO_H	NO	[--]

Table 4 – Calculation and verification of the Helmholtz cavity acoustic mode.

In annex A1 the calculations are reported for each side opening with gradually reduced flow rate for both operating condition and for the sensitivity upper and lower pressures.

7.2 Channel type oscillators

Two additional oscillation modes are considered as an approximation of the more complex acoustic modes extending between the former Helmholtz neck port and the top discharge side from the cooling channels.

The parallel channels of rectangular cross section of 20 x 3 mm (Fig. 23) are considered as stand-alone tubes having reflective open end boundaries.

The first two corresponding modes considered are therefore (Fig. 26):

1. one with the channel length L_{ap} equal to half a wavelength λ (two pressure nodes, at the bottom and top ends),
2. one with the channel length L_{ap} equal to one wave length λ (three pressure nodes, the former plus one at the mid point of the channel).

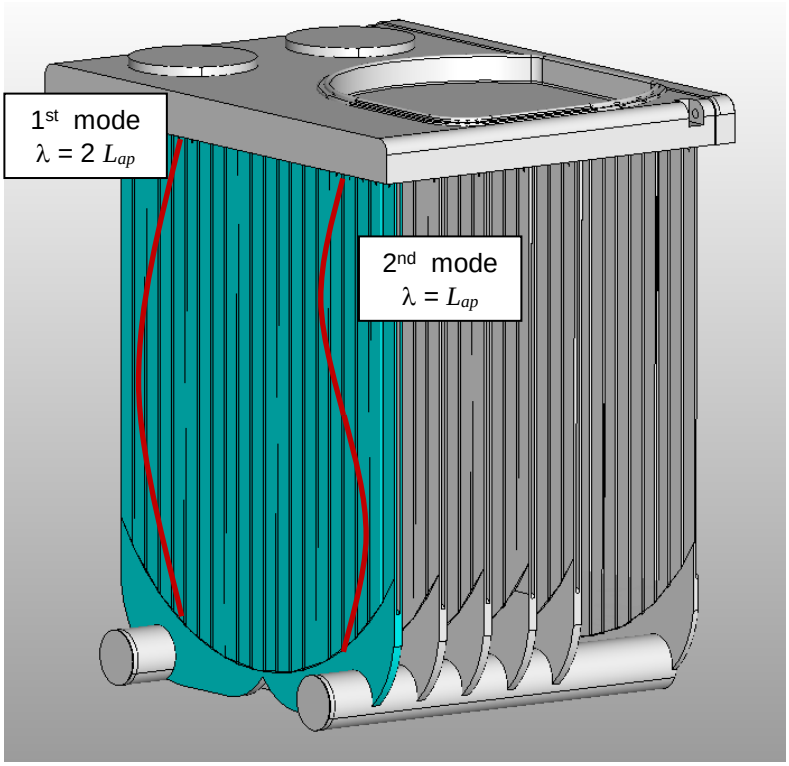

Fig. 26 – Representation of the first two channel resonant acoustic modes.

The length of the channel (550 mm) is taken as the average of the 21 pairs, which differ in length since their lower ends are enveloped by a circular arc (Fig. 20 lower). This assumption yields a conservative evaluation of the resonant pattern as the differing lengths of the parallel tubes would cause a smoother modal response due to the partly destructive interference among the respective standing waves. Should a more detailed analysis be necessary an acoustic model with parallel tubes of different length should be considered to verify this hypothesis.

The frequency of these two channel modes resonance is then given by the equations reported in Table 5, yielding the values for the first side opening, subject to the whole flow coming from the cradle inlet tube, i.e. 50% of the total cooling gas flow, under the operating condition A.

Table 5 shows the margin between the resonant frequency and the central vortex frequency, i.e. that at which maximum pulsation amplitudes are expected, derived from Table 3 and the result of the check of the necessary condition for lock-on. i.e.:

- That the resonant frequency falls within the min-max vortex frequency range ±20%

  AND

- That the Reynolds number of the grazing flow is greater than the minimum to self sustain the oscillation (10^5)

1st channel acoustic mode: $f_{\lambda/2} = \frac{c_s}{2L_{ap}}$	$f_{\lambda/2}$	317	[Hz]
Acoustic Margin (from Central vortex frequency)	$AM_{\lambda/2}$ *(center)*	-70%	[--]
Lock-on condition ($0.8 * f_{v,min} < f_{\lambda/2} < 1.2 * f_{v,max}$) AND ($Re > Re_{min}$)	$ALO_{\lambda/2}$	NO	[--]
2nd channel acoustic mode: $f_{\lambda/2} = \frac{c_s}{L_{ap}}$	f_{λ}	635	[Hz]
Acoustic Margin (from Central vortex frequency)	AM_{λ} *(center)*	-40%	[--]
Lock-on condition ($0.8 * f_{v,min} < f_{\lambda} < 1.2 * f_{v,max}$) AND ($Re > Re_{min}$)	ALO_{λ}	Ac. Lock-on	[--]

Table 5 – Calculation and verification of the channels resonance acoustic mode.

In annex A1 the calculations are reported for each side opening with gradually reduced flow rate for both operating condition and for the sensitivity upper and lower pressures.

8 STRUCTURAL MODES LOCK-ON CHECK

As last step of the FIV verification process, the frequency(ies) calculated above, subject to the condition that acoustic lock-on applies, are verified against the structural vibration modes, provided by the Client (Table 6).

For the example shown in the preceding section, relevant to the first anti-creep plate, subject to the whole flow coming from the cradle inlet tube, i.e. 50% of the total cooling gas flow, under the operating condition A, the result is that there is no structural lock-on between the only acoustic mode that can be self-excited (2nd channel acoustic mode), because the frequency of the latter (635 Hz) exceeds the range of the anti-creep plate modes provided.

Structural modes		Frequency [Hz]
Mode 1	$f_{s,1}$	50.3
Mode 2	$f_{s,2}$	64.7
Mode 3	$f_{s,3}$	119.1
Mode 4	$f_{s,4}$	130.0
Mode 5	$f_{s,5}$	168.5
Mode 6	$f_{s,6}$	180.3
Mode 7	$f_{s,7}$	206.7
Mode 8	$f_{s,8}$	271.2
Mode 9	$f_{s,9}$	299.9
Mode 10	$f_{s,10}$	317.7
FIV lock-on check		
Structural - acoustic - vortexes lock-on (Y/N)	Struct. Lock-on Check	N

Table 6 – Structural modes of the anti-creep plates and lock-on check for the example reported in the preceding tables.

9 RESULTS DISCUSSION

9.1 Outline of the results

The analysis above described by its steps has been performed by means of the spreadsheets that are part of the calculation report under annex A1.

The tables are identical as regards structure and equations, but differ by the gas pressure considered (1 ± 0.1 atm):

- Modes_lock_on_check_0.9 atm
- Modes_lock_on_check_1.0 atm
- Modes_lock_on_check_1.1 atm

From top to bottom they include all the steps illustrated in the preceding sections, for all the side openings going to each anti-creep plate, namely:

- geometric data and derived quantities
- fluid and operating data (flow rate, p and T) and derived properties
- vorticity calculations at cradle tube ports, as function of Strouhal number (min, central or of maximum pulsation amplitude, max), according to the quoted references in the notes.
- acoustic resonance calculations and acoustic-vortex lock-on check
- FIV lock-on check, i.e. synthesis of possible structural-acoustic-vortex lock-on.

The following figures show the synoptic results for each operating condition and pressure (1 atm, 0.9 atm, 1.1 atm) in which the abscissa corresponds to the mass flow rate, which varies along the fluid path, from the highest value corresponding the first opening, downstream the 90° bend, to the fifth through which 1/5 of the inlet flow rate passes.

The figures show the variation of the vortexes frequencies (solid lines) that cross the constant[7] acoustic resonant frequencies (dashed and dotted) to be read on the left axis and the variation of the Reynolds number to be read on the right axis.

The acoustic lock-on cases are highlighted by the frames overlapped.

[7] In theory the acoustic resonance frequencies would vary with the flow rate due to the damping that increases with the flow, but by a negligible amount.

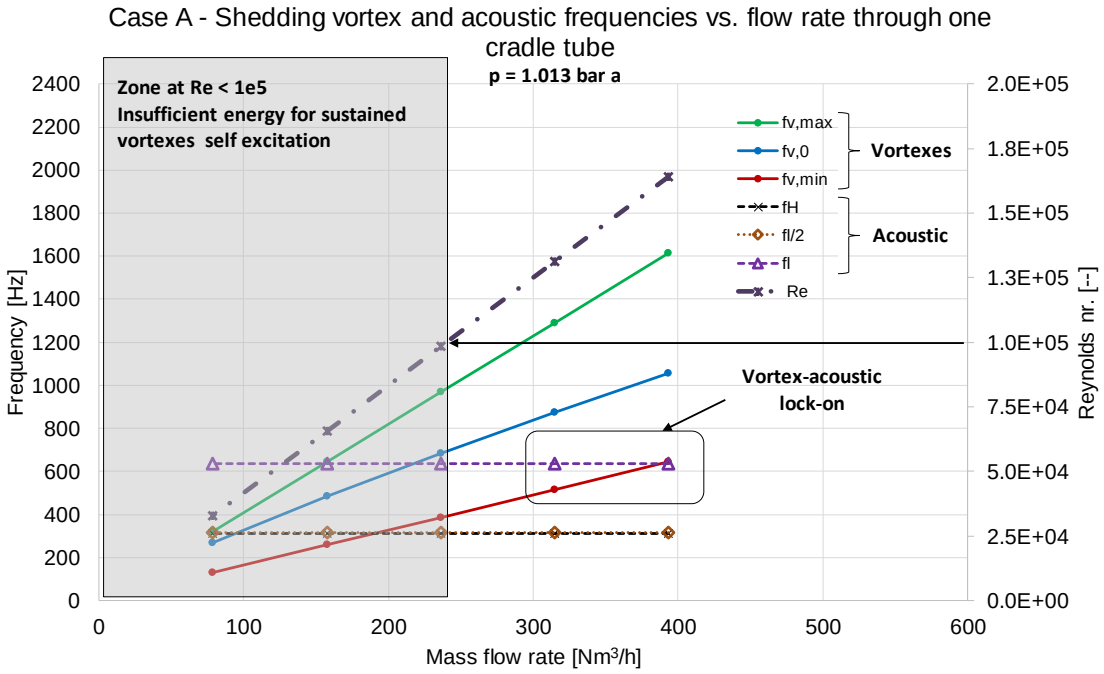

Fig. 27 – Synthesis of Case A at 1 atm pressure

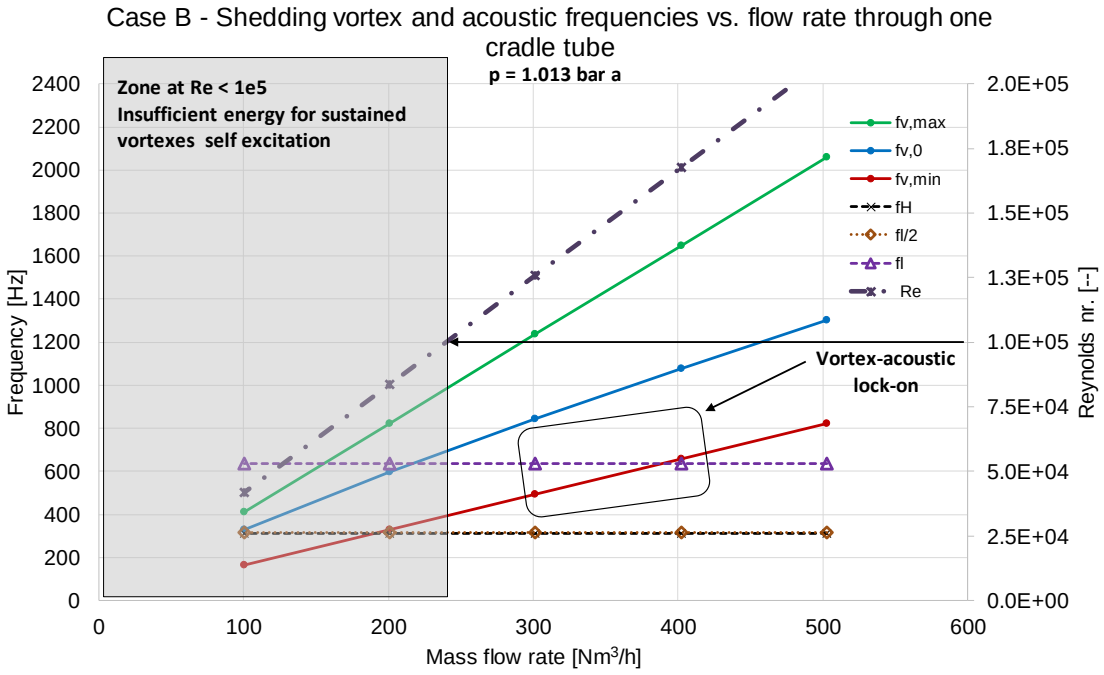

Fig. 28 – Synthesis of Case B at 1 atm pressure

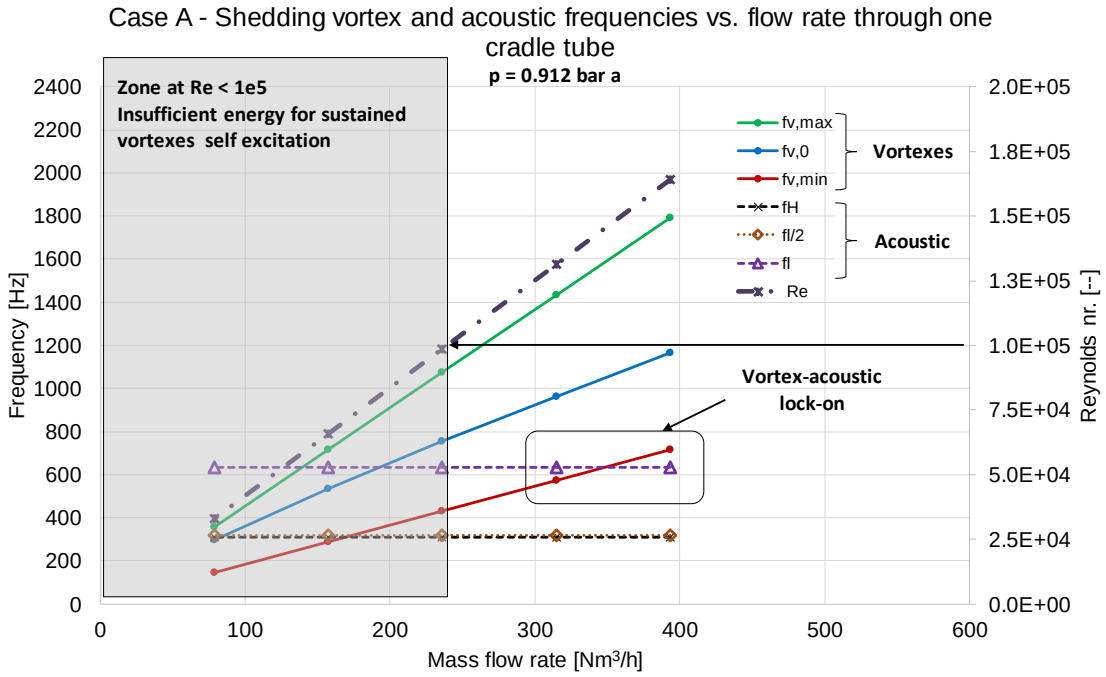

Fig. 29 – Synthesis of Case A at 0.9 atm pressure

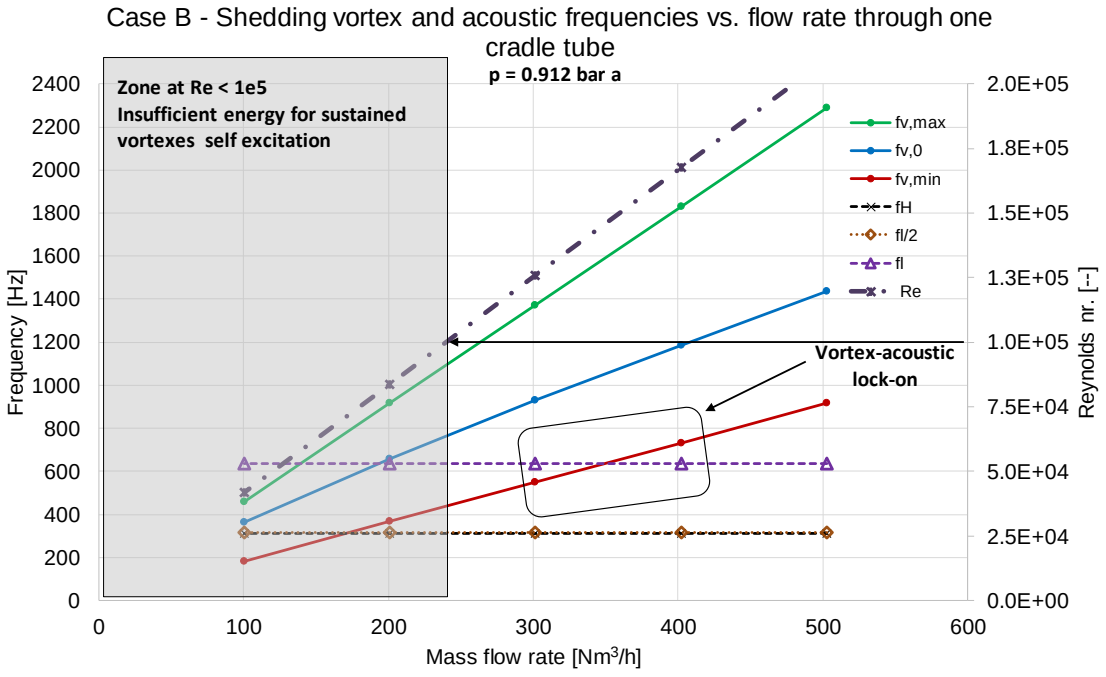

Fig. 30 – Synthesis of Case B at 0.9 atm pressure

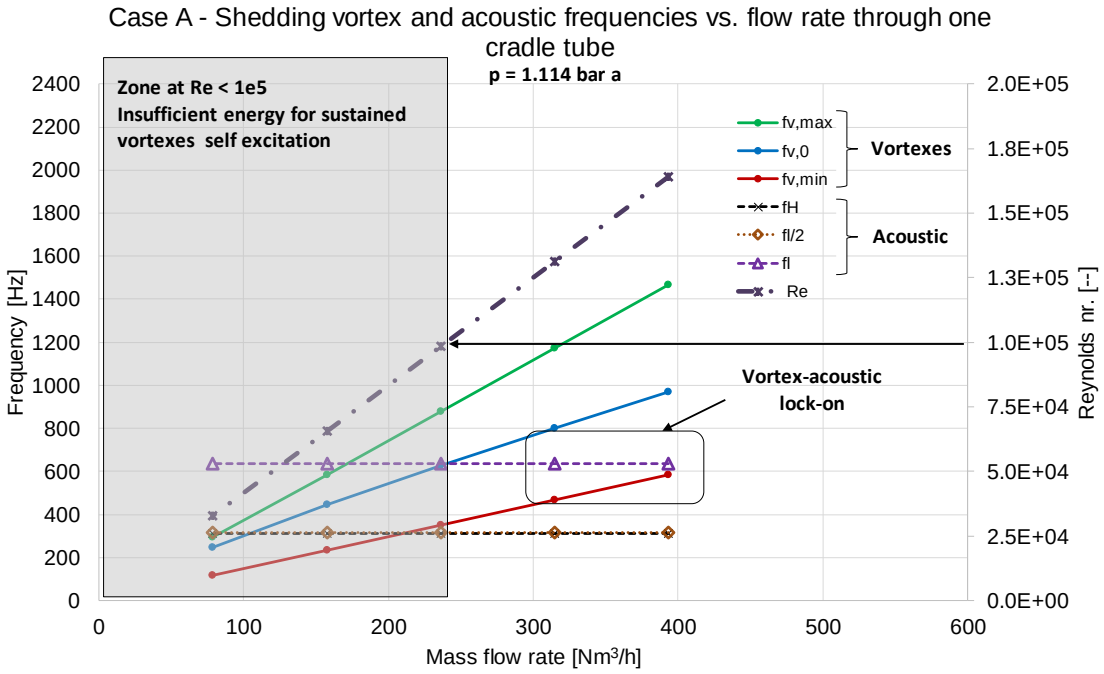

Fig. 31 – Synthesis of Case A at 1.1 atm pressure

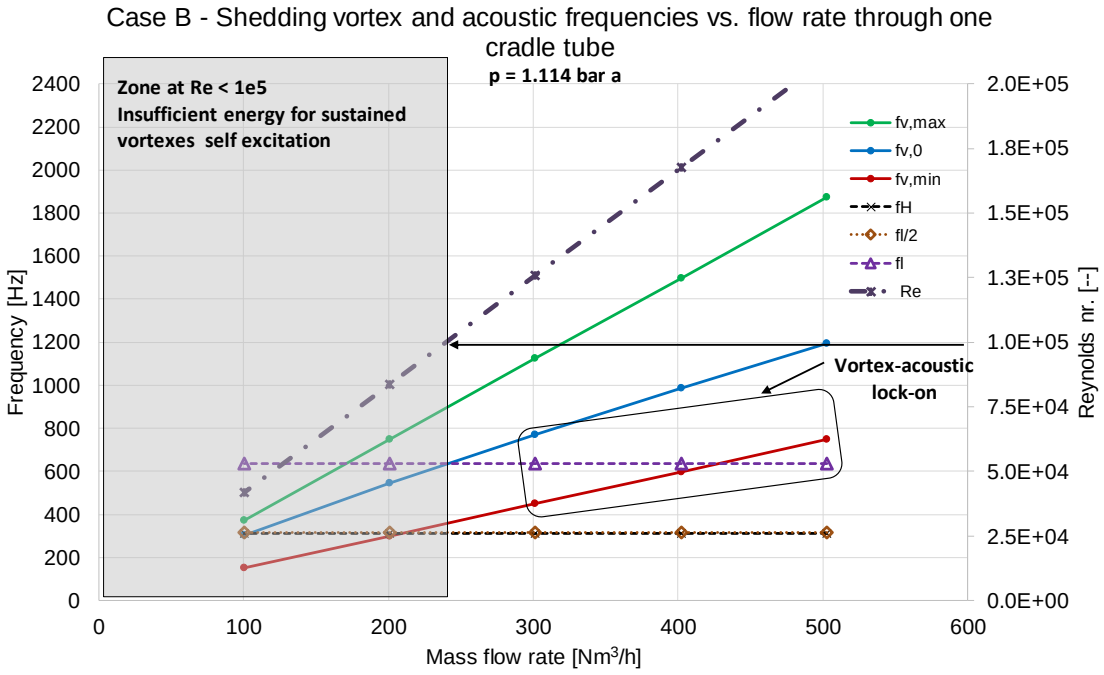

Fig. 32 – Synthesis of Case B at 1.1 atm pressure

9.2 Comments

The main observations arising from the figures analyses are the following:

1. The potential vortex frequency at the cradle ports openings span a range from about 130 Hz to about 2 kHz, depending on the operating condition (A or B) and on the port, out of the five channels rows at the base case pressure (1 atm).
2. However only in some of them the Reynolds number of the grazing flow exceeds the minimum value (10^5) needed to power self-excited standing waves by lock-on of acoustic modes, when theoretical frequencies match.
3. Moreover, above a certain grazing speed none of the three base acoustic modes considered (Helmholtz cavity, 1st and 2nd channels modes) would be locked to the vortex frequencies.
4. The Helmholtz type oscillator frequency and that of the first mode of the channel type are practically overlapped.
5. This restricts the potential acoustic-vortex lock-on frequencies to the range between about 500 Hz and 1.6 kHz in the base case pressure.
6. Only the 2nd channel type acoustic resonance, i.e. the one wave length mode ($L = \lambda$), of the vertical channels (at 635 Hz) could be excited by shed vortexes.
7. This possibility is however limited, at the base case pressure, to:
    a. the first two channels sets that are downstream the inlet of the cooling gas, in the operating case A
    b. to the 2nd and 3rd channel sets in the operating case B.
8. In no case the first ten structural modes of the anti-creep plates reported by the Client can lock-on to the above, since their maximum frequency (10th mode) is at about 318 Hz, thus far from the acoustic resonances with enough margin.
9. The results for the two other pressures, 0.9 and 1.1 atm, do not change substantially the above conclusions. The worse condition occurs, however, at the higher pressure for case B in which the first three anti-creep plate channels can resonate at the highest acoustic mode (635 Hz).
10. Finally it can be stated that the simplified analysis here presented, based on stand-alone Helmholtz cavities and channels models, does not hide possible lock-on of combined acoustic modes (i.e. spanning two or more channels), because these would have higher standing wave lengths, thus lower frequencies than those here obtained. In particular they would be lower than the vortex frequency range, and could match only at Reynolds numbers lower than the minimum needed to have enough power for self-sustained pulsations.

PAGE PURPOSELY BLANK

ANNEXES

PAGE PURPOSELY BLANK

A1. DETAILED CALCULATIONS

The following spreadsheet file report in detail the calculations and the sensitivity analysis performed.

610003-REP-WP4-T001 – Rev. 1 “n-Tof Target #3 - Preliminary Flow Induced Vibration analysis - detailed calculations”, dated 29/11/2018.

File: nTOF_Target#3_FIV_basis_01ab181129.pdf

PAGE PURPOSELY BLANK